121. Dendrimers with Porphyrin Cores: Synthetic Models for Globular Heme Proteins

by **Peter J. Dandliker, François Diederich*,** and **Adrien Zingg**

Laboratorium für Organische Chemie, Eidgenössische Technische Hochschule, ETH-Zentrum, Universitätstrasse 16, CH-8092 Zürich

and **Jean-Paul Gisselbrecht, Maurice Gross*,** and **Alain Louati**

Laboratoire d'Electrochimie et de Chimie Physique du Corps Solide, U.R.A. au C.N.R.S. no. 405, Faculté de Chimie, Université Louis Pasteur, 1 et 4, rue Blaise Pascal, F-67008 Strasbourg Cedex

and **Elizabeth Sanford**

Hope College, P.O. Box 9000, Holland, Michigan 49422-9000, USA

(16. VI. 97)

Dendritic iron porphyrins were synthesized as functional mimics of globular electron-transfer heme proteins. The cascade molecules **1** · **Zn**–**3** · **Zn** of first to third generation were obtained starting from the (*meso*-diarylporphyrin) zinc **6** · **Zn** which contains four carboxylate arms for attachment of the poly(ether-amide) dendritic branches by peptide-coupling methodology (*Scheme 1*). Generation 3 compound **3** · **Zn** with 108 methyl-carboxylate end groups has a molecular weight of 19054 D, and computer modeling suggests that its structure is globular and densely-packed, measuring *ca.* 4 nm in diameter and, therefore, similar in dimensions to the electron-transfer protein cytochrome-*c*. Starting from the generation 1 poly(carboxylic acid) **11** · **Zn** and the generation 2 analog **12** · **Zn** the dendritic Zn^{II} porphyrins **4** · **Zn** and **5** · **Zn**, respectively, were obtained by esterification with triethyleneglycol monomethyl ether (*Schemes 3* and *4*). Demetallation followed by insertion of Fe^{II} and *in situ* oxidation afforded the water-soluble dendritic iron porphyrins **4** · **FeCl** and **5** · **FeCl**. The electrochemical behavior of esters **1** · **Zn** – **3** · **Zn** in organic solvents changed smoothly with increasing dendritic generation (*Table 1*). Progressing from **1** · **Zn** to **3** · **Zn** in THF, the first porphyrin-centered oxidation and reduction potentials become more negative by 320 and 210 mV, respectively. These changes were attributed to strong microenvironmental effects imposed on the electroactive core by the densely packed dendritic surroundings. The electrochemical properties of **4** · **FeCl** and **5** · **FeCl** were investigated by cyclic voltammetry in both CH_2Cl_2 and H_2O (*Tables 2* and *3*). Progressing from **4** · **FeCl** to **5** · **FeCl** in CH_2Cl_2, the redox potential of the biologically relevant Fe^{III}/Fe^{II} couple remained virtually unchanged, whereas in aqueous solution, **5** · **FeCl** exhibited a potential 420 mV more positive than did **4** · **FeCl**. The large difference between these potentials in H_2O was attributed to differences in solvation of the core electrophore. Whereas the relatively open dendritic branches in **4** · **FeCl** do not impede access of bulk solvent to the central core, the densely packed dendritic superstructure of **5** · **FeCl** significantly reduces contact between the heme and external solvent. As a result, the more charged Fe^{III} state is destabilized relative to Fe^{II}, and the redox potential is strongly shifted to a more positive value.

1. Introduction. – Chemists have long hoped to mimic enzyme structure and function with synthetic systems [1]. By studying the subtle relationships between molecular structure and reactivity in relatively simple enzyme mimics, a great deal is learned about catalytic mechanisms in biological systems. Enhancing this understanding should permit scientists to engineer new generations of active and stable synthetic catalysts.

Historically, laboratory access to monodisperse macromolecules as large as natural enzymes was limited to synthetic polypeptides [2] whose secondary and tertiary structures

are highly complex and depend strongly on environmental factors such as solvent and temperature. Lacking diverse synthetic routes to very large, regular, non-peptidic structures, most organic chemists focused their enzyme mimetic efforts on small molecules, studying the effects of structural modifications near the synthetic active site on catalytic behavior [3]. Studies with low-molecular-weight enzyme mimics continue to provide valuable information about various aspects of enzyme mechanisms, but are incapable of evaluating certain unique influences which globular enzyme structure exerts on catalysis [4]. Since the globular shape and sheer bulk of enzymes contribute greatly to catalytic activity, such as by efficiently desolvating the active site, methods to mimic this globular structure would be valuable tools toward understanding enzyme function.

Cascade polymers (dendrimers) possess a well-defined topology based on the branched structure of trees [5] [6]. Efficient nonlinear growth schemes quickly provide high-molecular-weight, monodisperse globular structures with unique properties. By judicious choice of branched building blocks and functional-group chemistry, one can precisely control their shape, dimensions, density, polarity, flexibility, and solubility. Dendrimers can imitate the overall size and shape of naturally occurring proteins. Enzyme mimics based on dendrimers, being structurally simpler than enzymes, could conceivably be studied and analyzed more clearly than their natural counterparts. Delineating the effects of dendritic superstructure on catalytic properties could, therefore, enhance our mechanistic understanding of globular enzyme function.

Considerable research has been focused on introducing functional components on the exterior surface of dendrimers [6] [7] and within the dendritic branches [6] [8]. In contrast, when we started this investigation in 1990, the idea of incorporating initiator cores with well-defined functional properties had not been explored. At that time, we became interested in introducing apolar cyclophane binding sites [9] as well as porphyrins [10] as cores into globular dendrimers. Constructing a dendrimer around a porphyrin core could alter the polarity of the surroundings of the electrophore and modify its electrochemical behavior. Dendritic porphyrins could, therefore, be regarded as models for globular heme proteins such as cytochrome-*c*. The iron-heme moiety in these electron-transfer proteins exhibits oxidation potentials, in aqueous solution, 200–400 mV more positive than those of similarly ligated iron-heme model systems that lack the hydrophobic peptidic shell [11] [12]. Studies with dendritic mimics of heme-containing proteins promise to clarify the origins of the large changes in redox potential of the Fe^{III}/Fe^{II} couple in biological systems. With the recent 'exponential growth' [13] of dendrimer research, an increasing number of publications now describe the synthesis and properties of dendrimers with functional components located at the interior core [14]. Also, several investigations of dendritic porphyrins [15] and other redox-active dendrimers have appeared in the meanwhile [16] [17].

Here, we report the synthesis of two families of dendritic porphyrins, the Zn^{II} derivatives **1** · **Zn**–**3** · **Zn** of generations 1 to 3 [10a] and the water-soluble Fe^{III} derivatives **4** · **FeCl** and **5** · **FeCl** of generations 1 and 2, respectively [10b,c]. Extensive electrochemical studies reveal that the polarity around the redox-active chromophores at the interior core is efficiently controlled by the dendritic shells. These studies not only demonstrate that dendritic porphyrins represent suitable synthetic models of globular heme proteins; they also offer fascinating perspectives for modulating the characteristics of redox catalysts by means of dendrimer technology.

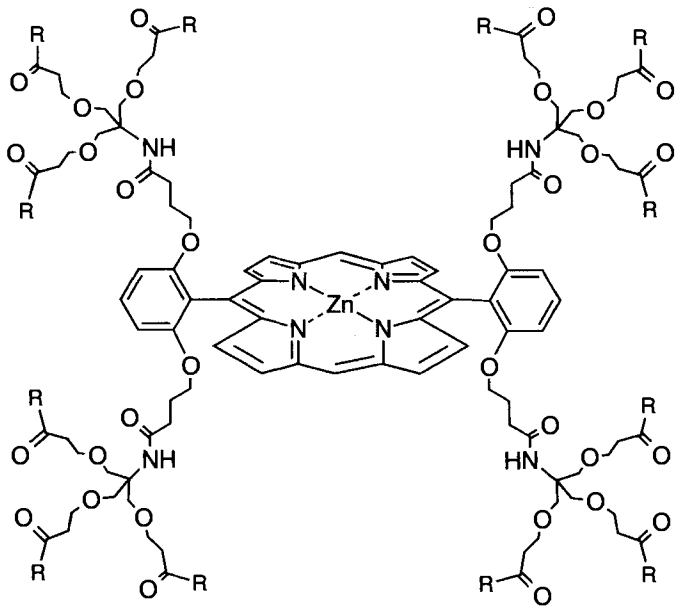

1•Zn R = OCH_3
11•Zn R = OH

2•Zn R = $NHC(CH_2OCH_2CH_2CO_2CH_3)_3$
12•Zn R = $NHC(CH_2OCH_2CH_2COOH)_3$

2. Results and Discussion. – 2.1. *Synthesis of the Dendritic Porphyrins.* The Zn^{II}-porphyrin tetracarboxylic acid **6 · Zn** was chosen as the initiator core for the construction of the cascade molecules. For the synthesis of **6 · Zn** (*Scheme 1*), 2,6-dihydroxybenzaldehyde [18] was alkylated with ethyl 4-bromobutyrate (*N*,*N*-dimethylformamide (DMF)/K_2CO_3) to give diester **7** in 65% yield. The *meso*-diarylporphyrin tetraester **9 · H_2** was constructed from **7** and di(pyrrol-2-yl)methane (**8**) [19] according to a protocol by *Manka* and *Lawrence* [20], and subsequent metal ion insertion yielded the Zn^{II} porphyrin **9 · Zn**. The longer-wavelength bands in the visible region of the electronic absorption spectra nicely reflected the successful insertion of the Zn^{II} ion [21] [22]: whereas **9 · H_2** displayed in CH_2Cl_2 four distinct bands at 502, 535, 578, and 633 nm, metallated **9 · Zn** only exhibited three characteristic bands in this region at 501, 539, and 576 nm. Successful metal-ion insertion was also revealed by the X-ray crystal structure of **9 · Zn** [10] (*Fig. 1*), which showed the four butyrate linkers suitably oriented above and below the porphyrin macrocyclic plane in the correct orientation for subsequent dendritic arm attachment. Hydrolysis finally afforded the initiator core **6 · Zn**.

The poly(ether-amide) cascade introduced by *Newkome et al.* [23] was chosen to generate the dendritic porphyrins **1 · Zn**–**3 · Zn** of first to third generation. When the porphyrin core **6 · Zn** and monomer **10** [23] were stirred in the presence of a large excess

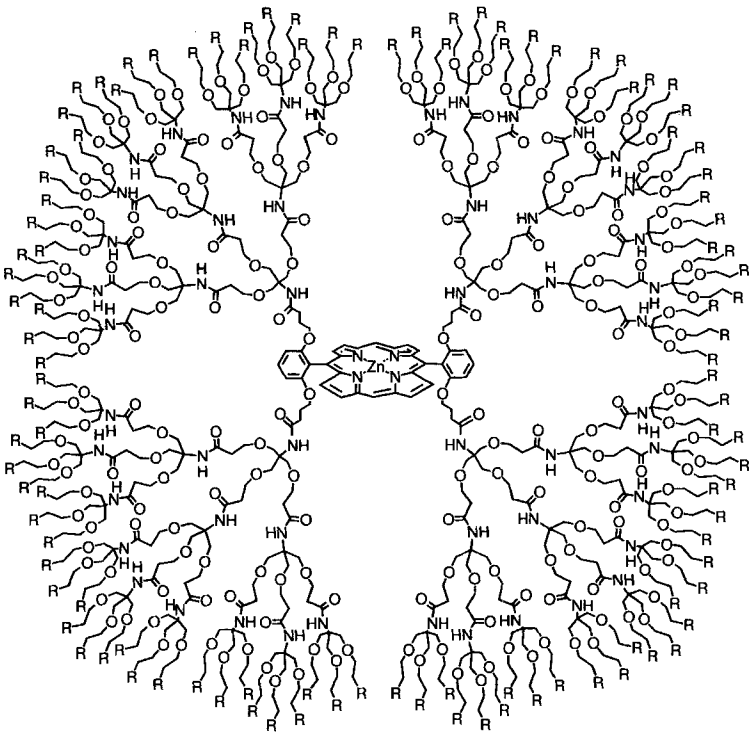

3•Zn R = $COOCH_3$

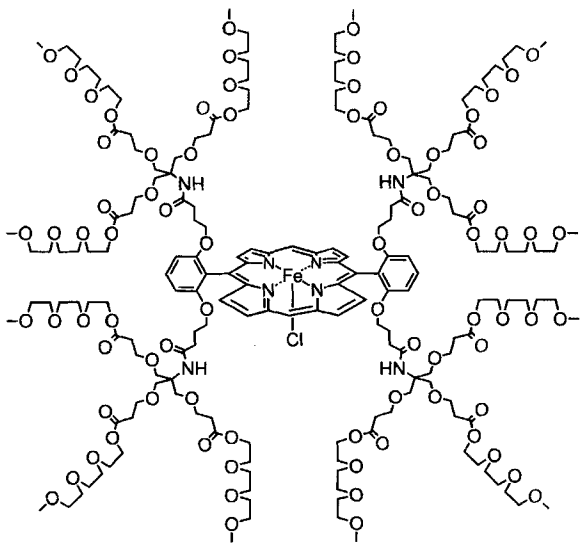

4•FeCl

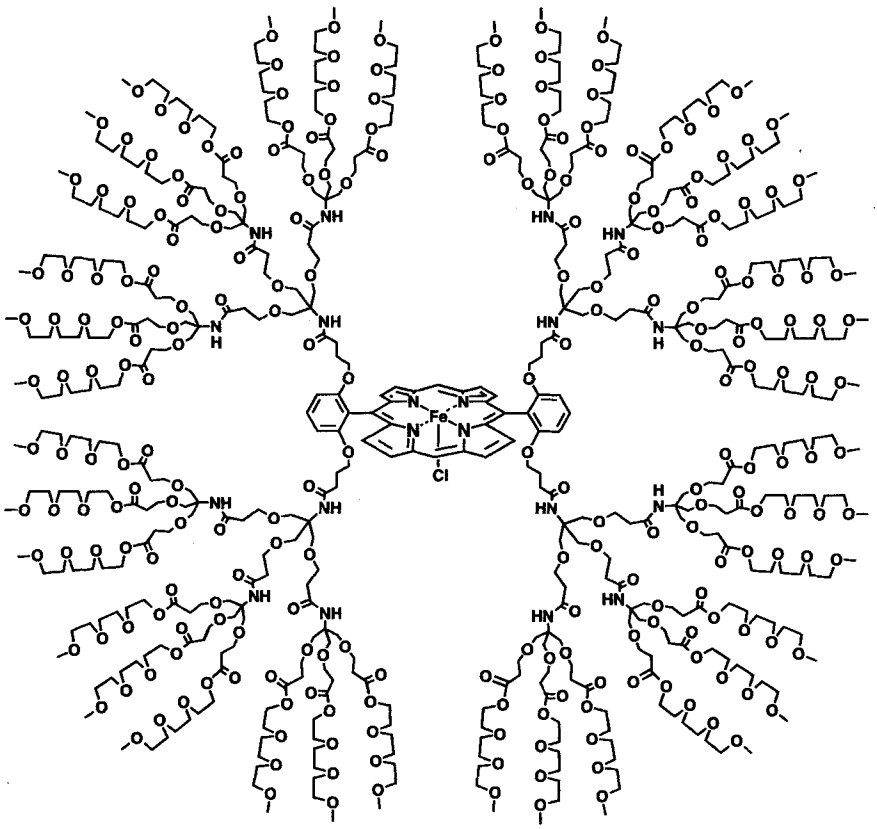

5•FeCl

of dicyclohexylcarbodiimide (DCC) and 1-hydroxy-1*H*-benzotriazole (BtOH) in 1,4-dioxane for 2 d, the first-generation dendritic Zn^{II} porphyrin **1 · Zn** with 12 ester end groups was obtained as a highly soluble, viscous red oil in 75% yield after purification by preparative gel permeation chromatography (GPC). Subsequent hydrolysis with LiOH in $MeOH/H_2O$ smoothly afforded the first-generation dodecacarboxylic acid **11 · Zn** (FAB-MS: 2211.1 (100%, MH^+, $^{12}C_{98}{}^{13}C_2H_{129}N_8O_{44}{}^{64}Zn$ requires 2211.7) as an amorphous red powder. Complete hydrolysis of **1 · Zn** was indicated by the ^1H- and ^{13}C-NMR spectra of **11 · Zn** in which the methyl-ester resonances had fully disappeared.

For the preparation of the second-generation dendrimer **2 · Zn**, dodecaacid **11 · Zn** was stirred for 18 h with monomer **10**, DCC, and BtOH in THF. Preparative GPC provided **2 · Zn** (mol.wt. 6548) bearing 36 methyl-ester end groups as a viscous red oil, whose ^1H-NMR spectrum was slightly broadened but still clearly exhibited all the characteristic resonances of the porphyrin core and the branches of first and second generation. Similarly, all observed ^{13}C-NMR resonances could be unambiguously assigned as shown in *Fig. 2*. The matrix-assisted laser-desorption-ionization time-of-flight (MALDI-TOF) mass spectrum of **2 · Zn** displayed the molecular ion as the base peak at

Scheme 1. *Synthesis of the Dendritic Zn^{II} Porphyrins* **1–3**

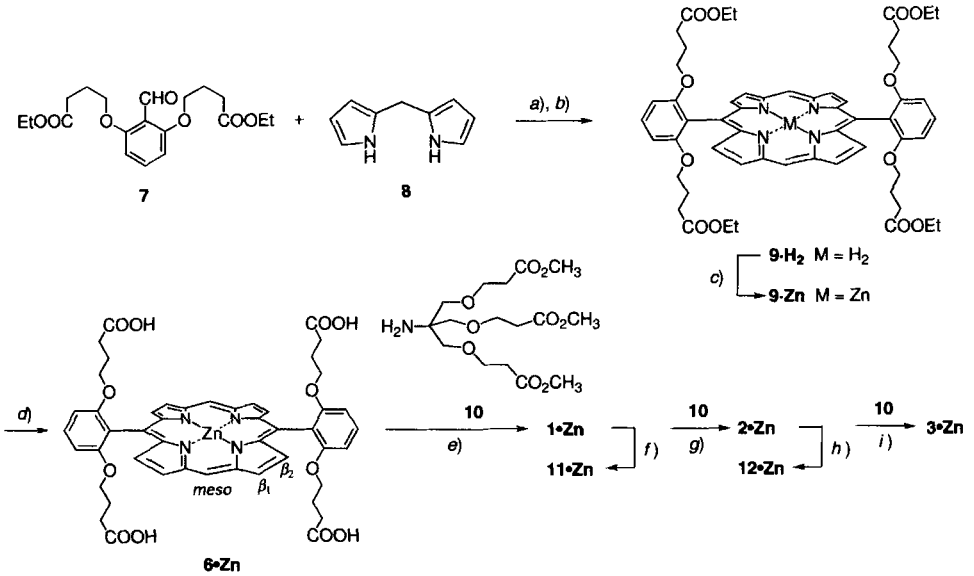

a) CF_3COOH, CH_2Cl_2, r.t., 18 h. *b*) *o*-Chloranil, CH_2Cl_2, Δ, 1 h, 43% (steps *a* and *b*). *c*) $Zn(OAc)_2 \cdot 2\,H_2O$, $CHCl_3$/MeOH 1:1, Δ, 30 min, 94%. *d*) Na_2CO_3, EtOH/H_2O 2:1, Δ, 15 h, 83%. *e*) DCC, BtOH, THF, r.t., 43 h, 75%. *f*) LiOH, MeOH/H_2O, r.t., 48 h, 81%. *g*) DCC, BtOH, THF, r.t., 18 h, 83%. *h*) LiOH, MeOH/H_2O 1:1, r.t., 48 h, 96%. *i*) DCC, BtOH, THF, r.t., 48 h, 51%.

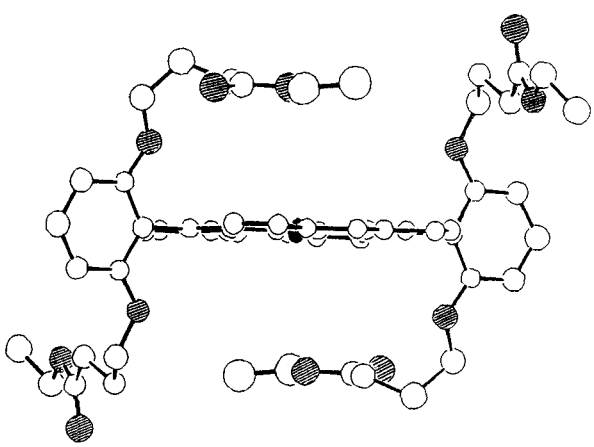

Fig. 1. *Molecular structure of* **9 · Zn** *in the crystal*

m/z 6547 ($^{12}C_{289}{}^{13}C_3H_{452}N_{20}O_{140}{}^{66}Zn$ requires 6547.8) in addition to a single minor peak at *m/z* 6200 with a relative intensity varying between 5 and 10% depending on the laser flux. Hydrolysis of the methyl-ester groups in **2 · Zn** was again accomplished with LiOH in MeOH/H_2O, yielding the solid second-generation derivative **12 · Zn** with 36 terminal COOH residues which was fully characterized by means of correct spectral and analytical data.

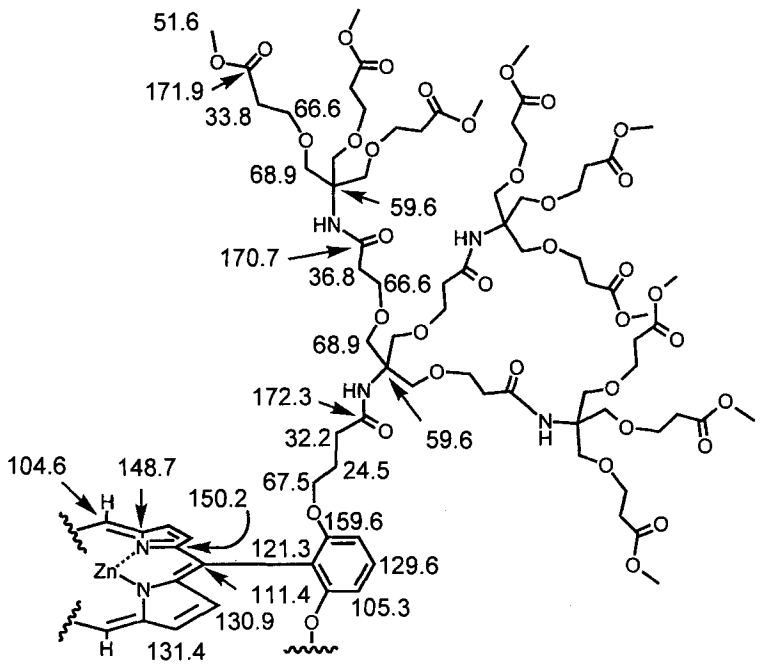

Fig. 2. *Assignment of the ^{13}C-NMR spectrum* (125 MHz, $CDCl_3$) *of the second-generation dendritic Zn^{II} porphyrin* **2 · Zn**

The third-generation dendritic porphyrin **3 · Zn** ($C_{832}H_{1352}N_{56}O_{428}Zn$, mol.-wt. 19053.55) with 108 terminal ester groups was finally obtained as a viscous red oil by coupling 36-acid **12 · Zn** with monomer **10** (*Scheme 1*). In the ^{1}H-NMR spectrum (500 MHz, $CDCl_3$) of **3 · Zn**, in addition to the resonances of first-to-third-generation dendritic branches, all the protons of the diarylporphyrin core were observed as strongly broadened 'singlets'. This is quite remarkable since the core protons represent only a small fraction of the total number of protons in the macromolecule. For example, the signal of the two *meso*-H-atoms at 10.00 ppm integrates only for 0.15% of the total 1352 H-atoms in **3 · Zn**. A nearly complete assignment of the resonances in the ^{13}C-NMR spectrum (125 MHz, $CDCl_3$) (*Fig. 3*) was possible. Except for the CH_2O and C=O resonances of the $O(CH_2)_3CONH$ linker arms to the diarylporphyrin core, which were buried underneath peaks for chemically similar C-atoms in the dendritic branches, all expected resonances were clearly discernible. Signals for the outermost tier (third-generation branching) were easily recognized due to their high intensity. As particular evidence for the high purity of the macromolecule, all 10 resonances of the diarylporphyrin core were clearly visible. The third-generation dendrimer **3 · Zn** with 108 methyl-ester end groups is monodisperse and pure according to ^{13}C-NMR spectroscopy. The MALDI-TOF-MS of **3 · Zn** depicted the broad molecular ion as the base peak at *m/z* 18900 ($^{12}C_{822}{}^{13}C_{10}H_{1352}N_{56}{}^{16}O_{427}{}^{18}O^{64}Zn$ requires 19052) together with minor peaks at around *m/z* 37000 and 54000, corresponding to ionic, gas-phase complexes of two and three molecules of **3 · Zn**, respectively.

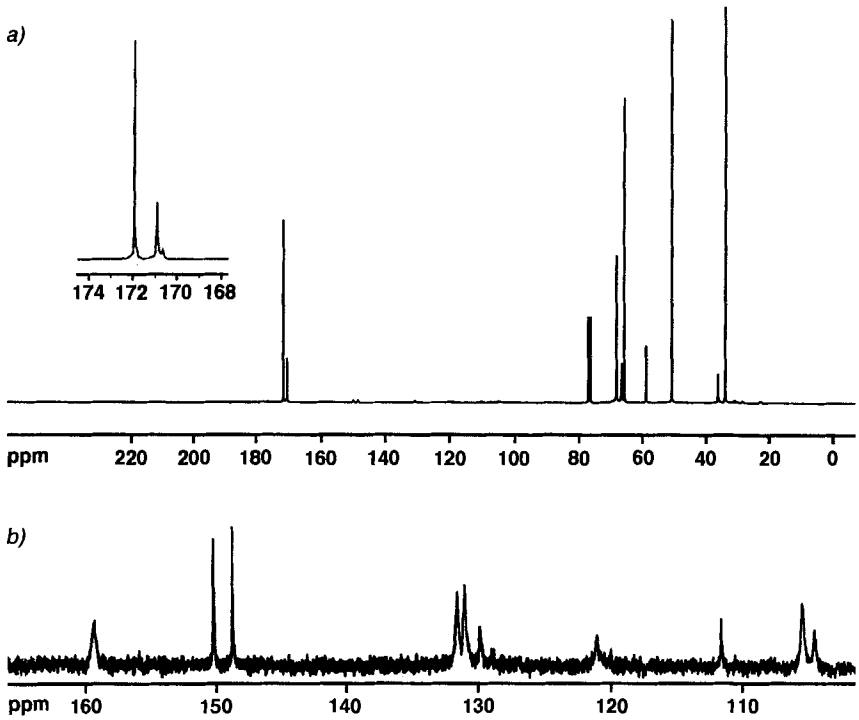

Fig. 3. a) *^{13}C-NMR spectrum* (125 MHz, $CDCl_3$) *of the third-generation dendritic Zn^{II} porphyrin* **3 · Zn**. The insert in the upper left corner shows the region of the carboxy C=O resonances. b) *Aromatic region of the ^{13}C-NMR spectrum of* **3 · Zn** *displaying all 10 resonances of the* meso-*diarylporphyrin core*

Computer-generated models of **3 · Zn** predicted a globular molecule, *ca.* 4 nm in diameter [10a]. The densely packed structure of **3 · Zn** resembles in size and shape the electron-transfer protein cytochrome-*c*, for which X-ray crystal structures revealed a globular structure with an encapsulated porphyrin core [24].

The cascade molecules **1 · Zn**–**3 · Zn** dissolve readily in common organic solvents and are, therefore, suitable for testing the influence of the dendritic shell on the redox potential of the Zn^{II} porphyrin in organic media. To extend such experiments into aqueous solution, it was necessary to functionalize the dendrimers with suitable end groups. For ease of product isolation and purification, we preferred uncharged solubilizing groups to charged ones. Furthermore, we wished at this stage to prevent possible strong influences of charged surface groups on the electrochemical properties of the core metalloporphyrin. To compare redox properties in both organic and aqueous solutions, we chose esters of triethyleneglycol monomethyl ether as end groups, since they should provide solubility in both environments. To further enhance the model character for globular heme proteins, the redox inactive Zn^{II} ion was to be replaced by the Fe^{III} ion.

Reaction of **6 · Zn** with DCC, BtOH, and triethyleneglycol monomethyl ether in THF readily provided tetraester **13 · Zn** (*Scheme 2*). Under similar reaction conditions, the free-base porphyrin **6 · H_2**, prepared by acid-mediated demetallation of **6 · Zn**, gave **13 · H_2**. The latter was then converted to the Fe^{III}-porphyrin chloride **13 · FeCl** with

$FeCl_2$ in THF. All three derivatives of **13** are viscous oils which dissolve in common organic solvents; however, they are insoluble in H_2O. The steric shielding provided by the four ester arms is apparently insufficient to block the π-stacking aggregation of the porphyrin surfaces and, ultimately, formation of stable crystal lattices.

Scheme 2. *Synthesis of the Porphyrin Tetraesters* **13 · Zn**, **13 · H_2**, *and* **13 · FeCl**

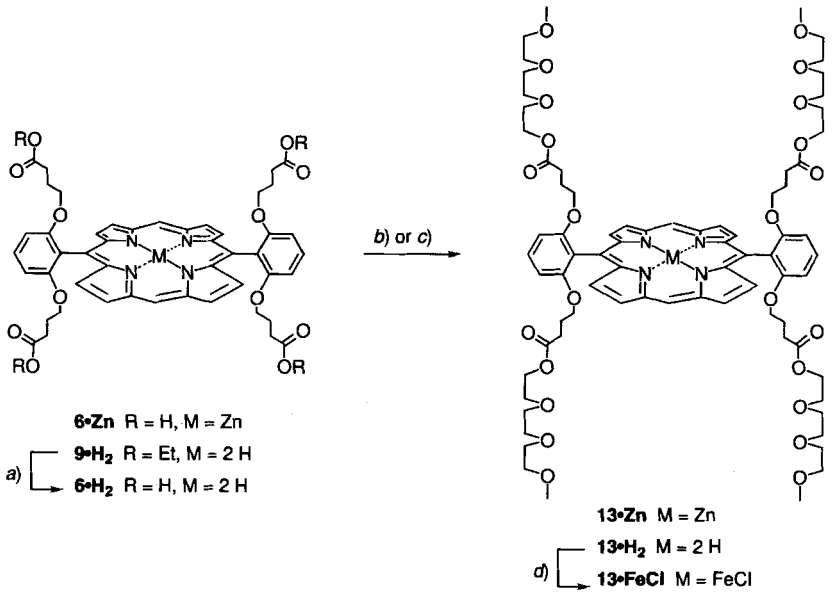

a) 1) Na_2CO_3, $EtOH/H_2O$, Δ, 2 d; 2) conc. HCl, 94%. *b*) DCC, BtOH, collidine, triethyleneglycol monomethyl ether, THF, r.t., 2 d, 74% (**6 · Zn** → **13 · Zn**). c) DCC, BtOH, collidine, triethyleneglycol monomethyl ether, THF, r.t., 2 d, 71%, (**6 H_2** → **13 H_2**). d) $FeCl_2$, THF, Δ, 1 h, 89%.

DCC/BtOH coupling of **11 · Zn** with triethyleneglycol monomethyl ether afforded dodecaester **4 · Zn** which, upon demetallation with 0.4M HCl, gave the free-base porphyrin **4 · H_2** (*Scheme 3*). The latter was transformed with $FeCl_2$ in refluxing THF into **4 · FeCl**, which was isolated as a brown oil. A similar sequence of reactions led from **12 · Zn** to **5 · Zn**, to **5 · H_2**, and finally to the second-generation dendritic Fe^{III} porphyrin **5 · FeCl** (*Scheme 4*).

The Zn/H exchange was confirmed by the appearance of ^{1}H-NMR signals at $\delta \approx -3.13$ ppm (pyrrole NH), the appearance of the four bands in the visible absorption spectrum characteristic of metal-free porphyrin, and correct mass spectral data. Compounds **4 · Zn**, **4 · H_2**, **5 · Zn**, and **5 · H_2** are all pure according to ^{1}H- and ^{13}C-NMR spectra. The successful introduction of the Fe^{III} ion yielding **4 · FeCl** and **5 · FeCl**, respectively, was confirmed by the characteristic UV/VIS spectrum for Fe^{III} porphyrins, ^{1}H-NMR signals for the β-pyrrole protons at $\delta \approx 13.2$ and 15.2 ppm, and the expected mass spectra. The MALDI-TOF mass spectrum of the first-generation dendritic Fe^{III}-porphyrin only displayed one peak for $[M - Cl]^+$ at m/z 3956.4 ($^{12}C_{182}{}^{13}C_2H_{296}N_8O_{80}{}^{56}Fe$ requires 3955.9), whereas the spectrum of the second-generation derivative showed the peak in the $[M - Cl]^+$ cluster at m/z 11297 ($^{12}C_{502}{}^{13}C_6H_{884}N_{20}O_{248}{}^{56}Fe$

Scheme 3. *Synthesis of the First Generation Dendritic Porphyrins* **4 · Zn**, **4 · H_2**, *and* **4 · FeCl**

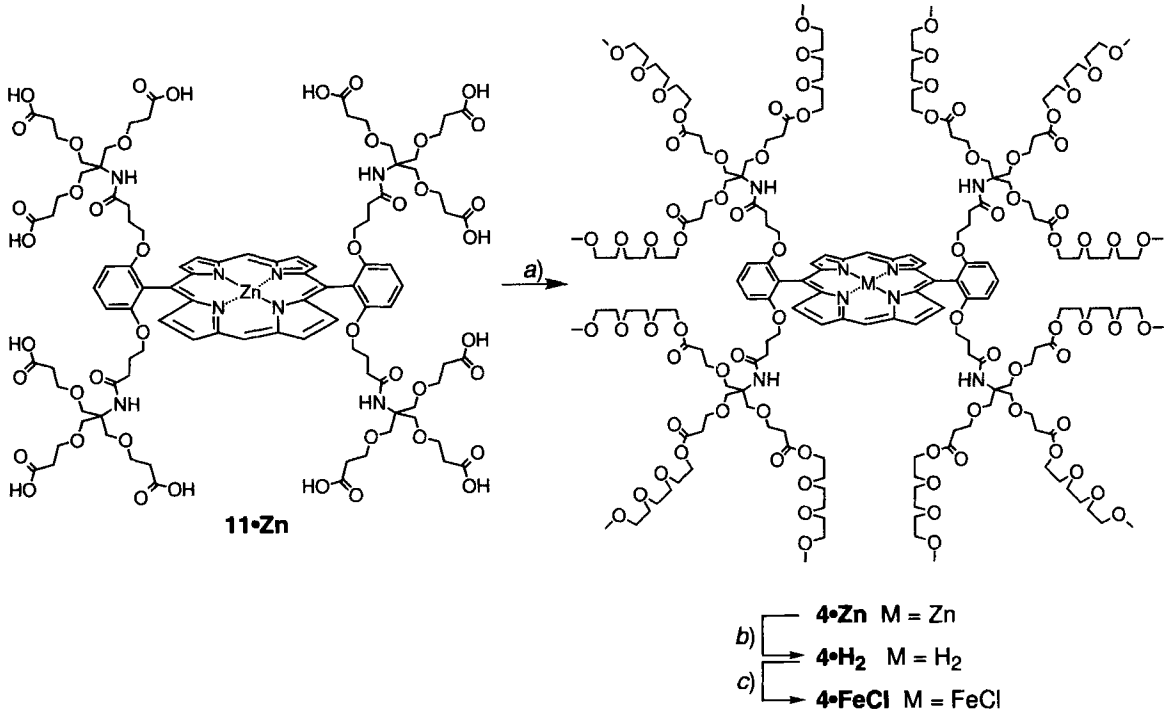

a) DCC, BtOH, collidine, triethyleneglycol monomethyl ether, r.t., 2 d, 92%. *b*) 0.4M aq. HCl, $CHCl_3$, r.t., 30 min, 93%. *c*) $FeCl_2$, THF, Δ, 1 h, 85%.

requires 11296) as the base peak besides a minor peak at *m/z* 10701. All first- and second-generation dendritic porphyrins with triethyleneglycol-monomethyl-ether end groups are viscous oils that dissolve remarkably well in solvents in the polarity range between water ($E_T(30)$ = 63.1) and *p*-xylene ($E_T(30)$ = 33.1) [25]. A simple extraction experiment demonstrated that H_2O solvates these dendrimers strongly, with a high kinetic barrier for desolvation. A bright pink solution of **4 · Zn** in CH_2Cl_2 was mixed with H_2O to give two phases. On standing for two days, the dendrimer remained completely in the organic phase. However, when a two-phase system containing an aqueous solution of **4 · Zn** and pure CH_2Cl_2 stood for several hours, virtually none of the dendrimer had partitioned into the organic phase which remained colorless. Only after standing for two days did the colored cascade molecule transfer completely into the CH_2Cl_2 layer.

2.2. *Electrochemical Investigations of the Dendritic Zn^{II} Porphyrins* **1 · Zn–3 · Zn** *in Organic Solutions: Strong Microenvironment Effects on Porphyrin-Centered Redox Processes.* In the first series of investigations, the influence of the specific microenvironment created by the dendritic superstructure in **1 · Zn–3 · Zn** on the redox potentials of the central Zn^{II}-porphyrin core was explored by cyclic voltammetry (CV). Since these dendrimers with methyl-carboxylate end groups are insoluble in H_2O, the electrochemical studies were conducted at 298 K in organic solvents such as CH_2Cl_2 or THF in the

Scheme 4. *Synthesis of the Second-Generation Dendritic Porphyrins* **5·Zn**, **5·H$_2$**, *and* **5·FeCl**

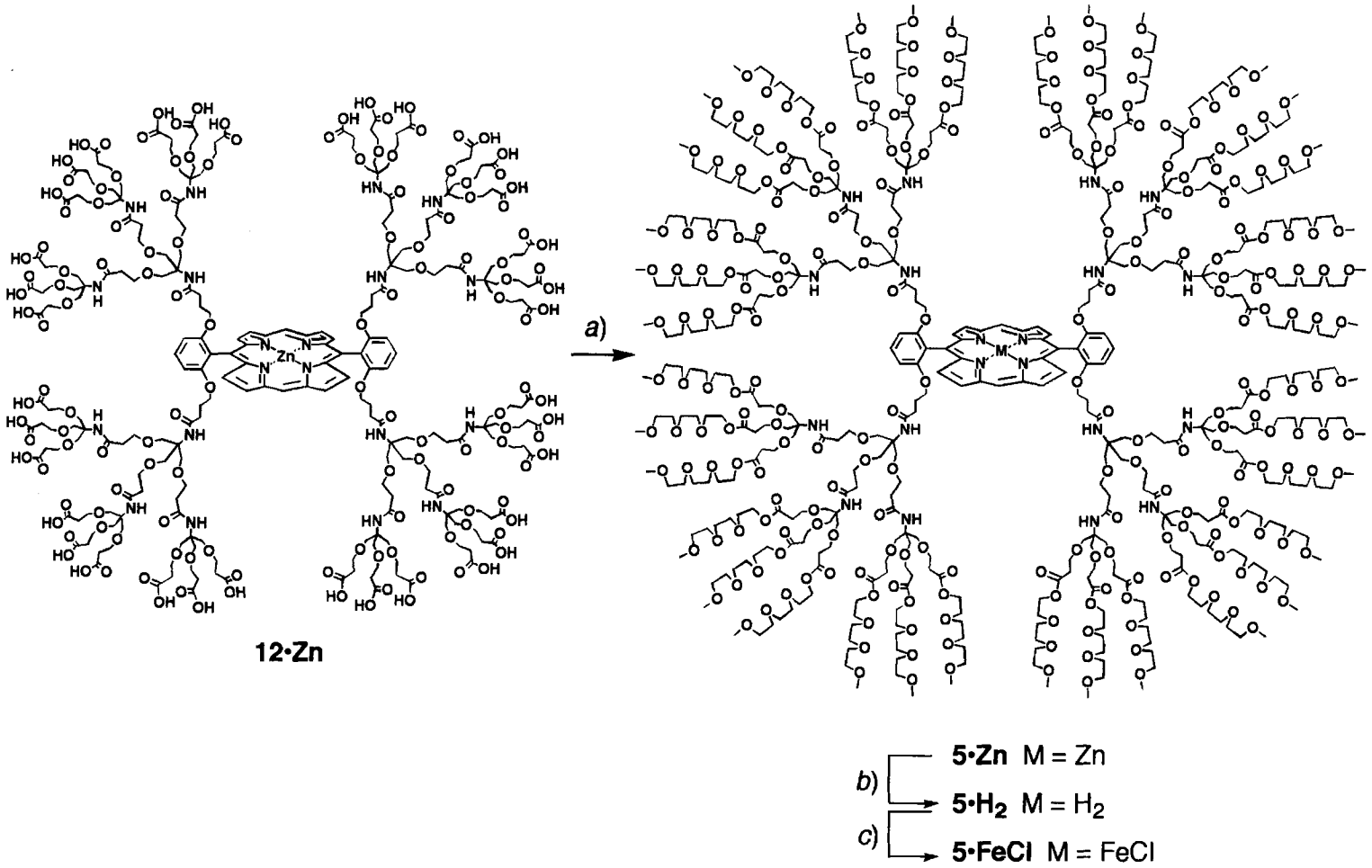

a) DCC, BtOH, collidine, triethyleneglycol monomethyl ether, r.t., 2 d, 80%. *b*) 0.4M aq. HCl, $CHCl_3$, r.t., 30 min, 88%. *c*) $FeCl_2$, THF, Δ, 1 h, 80%.

presence of Bu_4NPF_6 (0.1M) as supporting electrolyte. Reductions were performed at a dropping Hg electrode in THF (scan rate 5 V s^{-1}), while oxidations were performed at a Pt electrode in THF (scan rate 50 mV s^{-1}) or CH_2Cl_2 (scan rate 100 mV s^{-1}). All redox potentials E, approximated by $(E_p^a + E_p^c)/2$, are given in V *vs.* the standard calomel electrode (SCE). The Zn^{II} ion itself is electro-inactive and, within the accessible potential limit of the solvents, the majority of the observed electron-transfer processes were porphyrin-centered oxidations or reductions with only weak interference from the dendritic branches (see below). The redox potentials measured for dendrimers **1 · Zn**–**3 · Zn** in comparison to those of core structure **9 · Zn** and Zn^{II} *meso*-tetraphenylporphyrin are included in *Table 1*; examples of typical voltammograms are shown in *Fig. 4*.

Table 1. *Redox Potentials of Zn^{II} Porphyrins from Cyclic Voltammetry*[a])

Porphyrin	$E_{red}(I)$[b])	$E_{red}(II)$[b])	$E_{ox}(I)$[b])	$E_{ox}(I)$[c])	$E_{ox}(II)$[c])
Zn-TPP[d])	−1.50	−1.94	+1.08		
9 · Zn	−1.60	−2.01	+0.85	+0.63	+1.04
1 · Zn	−1.69	−2.18	+0.87	+0.71	+1.09
2 · Zn	−1.72	−2.18	+0.65	+0.63	+1.07
3 · Zn	−1.90[e])		+0.55[f])	+0.54	+1.00

[a]) E in V *vs.* SCE, approximated by $(E_p^a + E_p^c)/2$; supporting electrolyte Bu_4NPF_6 (0.1M), reductions performed at the dropping Hg electrode, scan rate 5 Vs^{-1}; oxidations performed at the Pt electrode, scan rate 50 mVs^{-1}; T = 298 K. [b]) Solvent THF. [c]) Solvent CH_2Cl_2. [d]) Zinc-*meso*-tetraphenylporphyrin (Zn-TPP). [e]) Poorly defined signal. [f]) Broad signal.

The first- and second-generation compounds **1 · Zn** and **2 · Zn** exhibited two reversible one-electron reduction processes between −1.0 and −2.5 V *vs.* SCE. The absolute potential difference between the first and the second reduction potentials was 0.49 and 0.46 V, respectively. These values are in good agreement with the 0.35 to 0.40 V range typically observed for macrocycle-centered reductions of metalloporphyrin complexes [26]. The third-generation compound **3 · Zn** showed a less well defined wave for a single irreversible reduction process which, in dilute solutions, was located at *ca.* −1.9 V (*Fig. 4, a*). Control experiments with **14** suggested that signals for the electrochemical reduction of the Zn^{II} porphyrin in **3 · Zn** are overlapped in the region from −1.6 V to the accessible potential limit of the solvent by broad irreversible multi-electron-transfers to the dendritic branches.

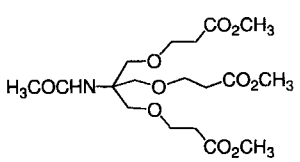

14

The first reduction potential of the Zn^{II} porphyrin becomes more negative with increasing dendrimer generation. The values obtained for **1 · Zn**–**3 · Zn** are by 90 to 300 mV more negative than the potential required for the reduction of the porphyrin macrocycle in the simple core structure **9 · Zn**. These results suggest that the overall effect

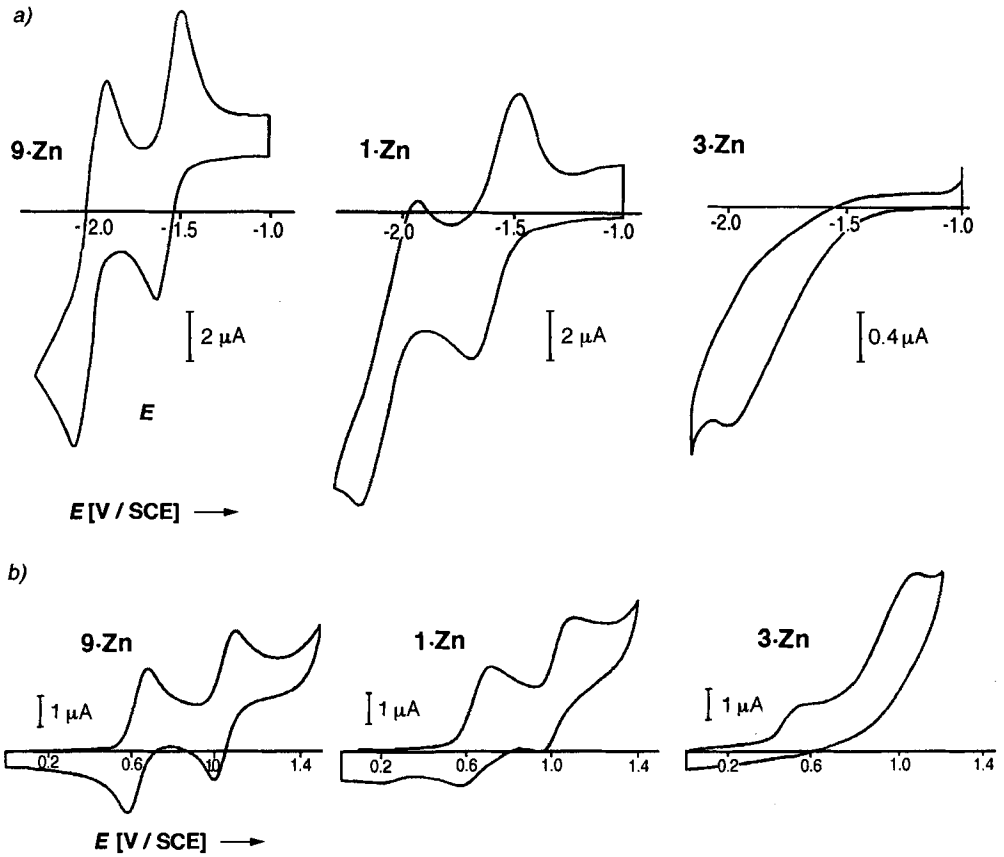

Fig. 4. *Cyclic voltammograms of* **9 · Zn**, **1 · Zn**, *and* **3 · Zn** *at 298 K. a*) Reduction in THF (+ 0.1M Bu_4NPF_6); dropping Hg working electrode, scan rate 5 V s^{-1}. *b*): Oxidation in CH_2Cl_2 (+ 0.1M Bu_4NPF_6); Pt working electrode, scan rate 100 mVs^{-1}.

of the poly(ether-amide) dendrimer shell is to make the microenvironment around the central porphyrin ring more electron rich with increasing generation. The numerous O-atoms of the dendritic branches apparently tend to destabilize a negative charge on the porphyrin [27], making its reduction energetically more difficult with increasing dendrimer generation.

A similarly strong microenvironmental effect was observed in the oxidation of **1 · Zn**–**3 · Zn** as compared to the core compound **9 · Zn**. At the Pt electrode between 0 and 1.2 V, the first- and second-generation dendrimers **1 · Zn** (*Fig. 4, b*) and **2 · Zn** displayed two reversible oxidation steps in CH_2Cl_2, whereas only one was observed in THF before reaching the anodic solvent-accessible potential limit. It should be noted that the two oxidation processes in CH_2Cl_2 are less reversible than those generally observed for other metalloporphyrins in aprotic solvent [26]. For the third generation dendrimer **3 · Zn**, the two oxidation processes that were observed in THF became completely irreversible in CH_2Cl_2 (*Fig. 4, b*). Control compound **14** did not show any oxidation

signal in either solvent up to the anodic potential limit. In all three dendritic systems, electrochemical oxidation should generate monocations in which the electron is removed from the porphyrin π-system. Evidence for this assignment comes from the potential difference between the first reduction and the first oxidation which varies between 2.37 and 2.56 V, values comparable to the 2.25 $\pm$ 0.15 V separation reported for other metalloporphyrin complexes [26]. In the dendritic complexes, the first oxidation potentials are up to 300 mV (THF) less positive than that of core compound **9** · **Zn**. This can again be explained by the increasingly electron-rich microenvironment provided by the dendritic branches, which now favors the generation of the porphyrin radical cation.

In contrast to through-bond substituent effects that are traditionally used to influence the electrochemical behavior of metalloporphyrins, a through-space mechanism modulates the redox characteristics of **1** · **Zn**–**3** · **Zn** by controlling the polarity of the environment around the electrophore. Upon increasing the thickness and density of the dendritic branching in this series, however, the chemical irreversibility of both reduction and oxidation processes increases. This phenomenon is at present not well understood [17g]. Furthermore, whereas the explanation of the changes in reduction potentials by changes in the micropolarity around the core electrophore is an attractive one, it cannot be entirely excluded that differences in the accessibility of counterions from the electrolyte to the porphyrin core in **1** · **Zn**–**3** · **Zn** could cause part of the observed differences in reduction potential. Thermodynamic and kinetic host-guest binding studies with arene or steroid binding dendrimers of similar size and structure [9b–d], however, strongly suggest that the density of the branching, even at the stage of the third-generation compound, is not sufficient to prevent rapid penetration of counterions and individual solvent molecules on the time scale of the CV experiments.

Independent of their exact microscopic origin, the observed potential changes clearly show that with increasing dendritic generation, the central porphyrin increasingly encounters an environment that differs from bulk solvent. This is further demonstrated by the comparison of the oxidation potentials measured for **1** · **Zn**–**3** · **Zn** in THF and CH_2Cl_2. The plot of the first oxidation potential *vs.* dendrimer generation (*Fig. 5*) shows that at the first generation, the potentials in both solvents differ significantly. At this stage, the core porphyrin apparently is still exposed to the polarity of the bulk solvent. At the second generation, the thicker, denser dendritic shell increasingly prevents exposure of the porphyrin to bulk solvent. Hence, the oxidation potentials not only are strongly shifted, as compared to the stage of the first generation, but they become similar in both solvents, differing only by 20 mV. At the third generation, this difference narrows to only 10 mV. Clearly, at the higher generations, the dendrimer itself is acting as a covalently attached solvent cage for the central porphyrin.

2.3. *Electrochemical Investigations of the Dendritic Fe^{III} Porphyrins* **4** · **FeCl** *and* **5** · **FeCl**. – 2.3.1. *Parameters Affecting the Reduction Potential of Heme Proteins.* The potential of the biologically relevant Fe^{III}/Fe^{II} couple in electron-transfer heme proteins depends on a variety of parameters such as the electronic character of heme substituents, the nature of the axial ligands to the metal ion, electrostatic interactions between the heme and charged protein residues and ions, and the polarity of the microenvironment around the porphyrin. Synthetic model systems have frequently been used to quantify the subtle relationships between structural and environmental factors and reduction potential. Generally, electron-rich substituents on the porphyrin stabilize the Fe^{III} state and

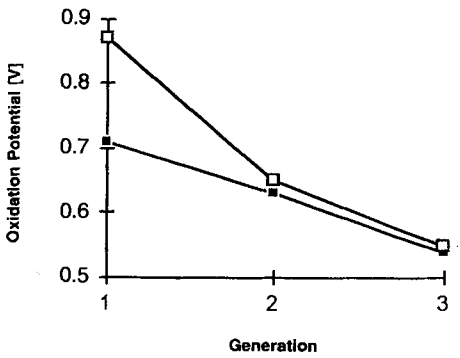

Fig. 5. *Plot of the First Oxidation Potential* vs. *Dendrimer Generation in THF* (upper curve) *and* CH_2Cl_2 (lower curve) *for the Dendritic* Zn^{II} *Porphyrins* **1** · **Zn**, **2** · **Zn**, *and* **3** · **Zn**. The data are taken from *Table 1*.

shift the potential of the Fe^{III}/Fe^{II} couple by 10–100 mV to more negative values [28]. Substituent effects on the reduction potentials of free-base porphyrins have also been extensively investigated [29]. Variations of the nature of the axial ligands have been shown to shift the Fe^{III}/Fe^{II} reduction potential by up to several hundred mV both in model systems [30] and in cytochrome-*c* mutants obtained by site-directed mutagenesis [31]. Thus, replacement of Met80, which together with a His residue acts as an axial ligand in the wild-type enzyme, by a His80 lowers the potential of the Fe^{III}/Fe^{II} couple by 221 mV. Protein and model-system investigations both show that electrostatic interactions between the buried heme redox center with protein surface charges affect the potential [32] as does the H-bonding between axially ligated imidazoles and neighboring residues [33].

The polarity of the heme microenvironment has a particularly large influence on the reduction potential of the Fe^{III}/Fe^{II} couple [4]. Thus, the reduction potential of the Fe^{III}/Fe^{II} couple in cytochromes is more positive by 200–400 mV [11][12] than that of similarly ligated, more solvent-exposed heme model compounds. For example, this couple in cytochrome-*c* is shifted by 200–300 mV to more positive potential, compared to a cytochrome-*c* heme octapeptide, obtained by partial digestion of the native protein. The apolar heme pocket in the native enzyme destabilizes the Fe^{III} state, thereby shifting the potential to more positive values. *Kassner* [4] developed a theoretical model which predicts the shift of the Fe^{III}/Fe^{II} redox potential for hemes buried in an apolar environment as a function of the polarity of this environment and the thickness of the hydrophobic polymer shell around the electrophore. This model nicely reproduced the shifts to more positive potential encountered in cytochromes. We applied it to predict the positive shift of the Fe^{III}/Fe^{II} redox potential in the dendritic porphyrin **5** · **FeCl** in H_2O by using values of 15–17 Å for the radius of the apolar dendritic shell (estimated from energy-minimized gas-phase structures of **5** · $\mathbf{H_2}$) and by assuming a polarity around the electrophore similar to that in naturally occurring proteins [34] and polyamide polymers such as *Nylon* [35]. These calculations estimated shifts of the Fe^{III}/Fe^{II} couple in **5** · **FeCl** of *ca.* 300–400 mV to more positive potential as compared to bulk solvent-accessible hemes [36].

2.3.2. *Electrochemical Studies of* **4 · FeCl** *and* **5 · FeCl** *in Organic Solution.* The effects of bulky superstructure on the electrochemical properties of iron porphyrins have been studied extensively in organic solvents by *Momenteau* and co-workers [27] [37]. They synthesized bridged 'basket-handle' iron porphyrins in which the bridging chains, containing ether or amide groups, were linked directly over the π-faces of the metalloporphyrin. The amide-containing chains sterically hindered the approach of bulk solvent and counterions to the porphyrin and also exerted a marked through-space electrostatic effect, shifting the half-wave potential of the Fe^{III}/Fe^{II} couple to more positive values. Given the steric bulk of the dendritic shell and the high local density of polar amide groups near the porphyrin ring in **4 · FeCl** and **5 · FeCl**, similar effects were expected to operate in these systems.

Cyclic voltammetry in CH_2Cl_2 (+ 0.1M Bu_4NPF_6) using a glassy carbon working electrode showed irreversible behavior for the Fe^{III}/Fe^{II} couple in **13 · FeCl**, typical of Fe^{III}-porphyrin chlorides, and consistent with equilibrated dissociation of the chloride counterion from the metal ion during electroreduction (*Fig. 6*) [38]. In contrast, both **4 · FeCl** and **5 · FeCl** showed reversible behavior for the Fe^{III}/Fe^{II} couple at −10 and +70 mV *vs.* SCE, respectively (*Fig. 6*, *Table 2*).

Both **13 · FeCl** and **4 · FeCl** displayed a one-electron oxidation step at + 1.06 V and a one-electron reduction step from Fe^{II} to Fe^{I} at −1.29 and −1.27 V, respectively, typical values for iron porphyrins (*Table 2*). The potential difference between the oxidation at +1.06 V and reduction to Fe^{I} was within the normal value of 2.25 ± 0.15 V reported for other metalloporphyrin complexes [26]. Compound **5 · FeCl** underwent reduction from Fe^{II} to Fe^{I} at −1.46 V, a potential that is 170 mV more negative than the corresponding one in reference compound **13 · FeCl**. This energetically less favorable metal-centered reduction with increasing dendrimer size is analogous to the increasingly difficult porphyrin-centered reduction observed in CH_2Cl_2 upon changing from **1 · Zn**, to **2 · Zn**, and to **3 · Zn** (*Table 1*).

To assign the observed cyclic voltammetric signals to particular redox reactions of the core iron porphyrin, spectroelectrochemical studies were performed using a Pt grid working electrode in CH_2Cl_2 (+ 0.1M Bu_4NPF_6). During the first reduction step at a controlled potential of −0.9 V *vs.* SCE, compound **4 · FeCl** exhibited well-defined isosbestic points, and the absorption spectrum remained characteristic of an iron porphyrin with only small changes in the position of the *Soret* and *Q* bands (*Fig. 7,a*). Similar spectral evolutions were observed for **13 · FeCl** when the electrolysis was carried out at the same electrolysis potential. Following the second reduction step at a controlled potential of −1.6 V *vs.* SCE, the spectrum of **4 · FeCl** remained typical for a metalloporphyrin, displaying red shifts of 20 nm for the *Soret* band and 16 nm for the *Q* band (*Fig. 7,b*). This behavior is characteristic of successive metal-centered reductions from Fe^{III} to Fe^{II} and subsequently to Fe^{I} porphyrins. Following the first reduction step, the initial spectra of **13 · FeCl** and **4 · FeCl** were both fully recovered after electrolysis at + 0.3 V. On the other hand, after the second reduction step, the initial spectrum could not be recovered by reoxidation due to the negative applied potential. Compound **5 · FeCl** exhibited analogous behavior, confirming that the first reduction step corresponded to the Fe^{III}/Fe^{II} couple. However, the presumed generation of an Fe^{I} species during the second reduction step at −1.46 V *vs.* SCE could not be monitored, since it occurred too close to the accessible cathodic potential limit of the solvent.

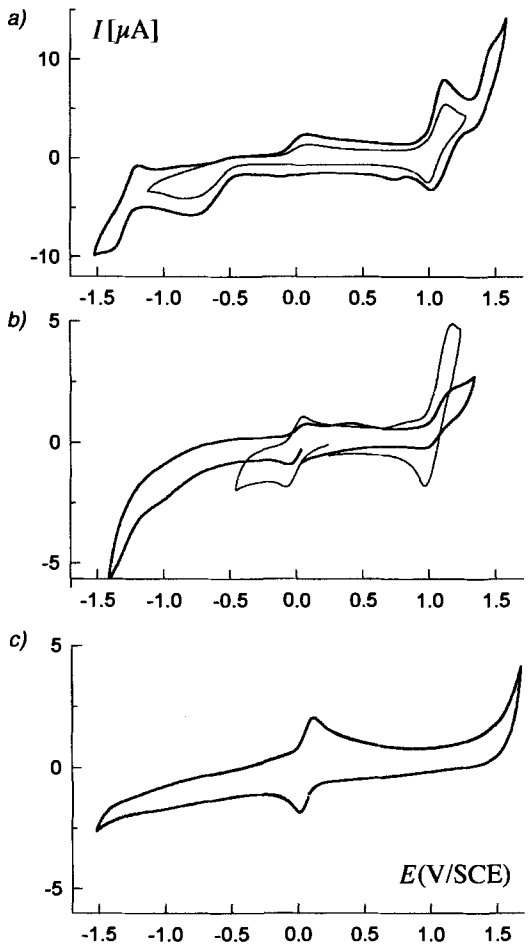

Fig. 6. *Cyclic voltammograms in* CH_2Cl_2 (+ 0.1M Bu_4NPF_6) *on a glassy carbon working electrode of* a) **13 · FeCl** *at 0.5* Vs^{-1} *for two different potential ranges,* b) **4 · FeCl** *at 0.1* Vs^{-1} (thick line) *and at 0.5* Vs^{-1} (thin line), *and* c) **5 · FeCl** *at 0.5* Vs^{-1}

Table 2. *Redox Potentials of the Dendritic Iron Porphyrins in* CH_2Cl_2[a])

Porphyrin	$E_{Fe^{II}/Fe^{I}}$	$E_{Fe^{III}/Fe^{II}}$	E_{ox}
13 · FeCl	−1.29[b])	−0.59[c])[d])	+1.06[b])
		+0.12[c]) [e])	
4 · FeCl	−1.27[c])	−0.01[f])	+1.06[b])
5 · FeCl	−1.46[c])	+0.07[f])	–

[a]) Reduction potentials in CH_2Cl_2 determined by cyclic voltammetry (CV): E (approximated by $(E_p^a + E_p^c)/2$) in V *vs.* SCE; supporting electrolyte 0.1M Bu_4NPF_6; glassy carbon working electrode, scan rate = 0.1 Vs^{-1}, T = 293 K. [b]) Quasi-reversible transfer. [c]) Irreversible transfer, peak potential from CV. [d]) Cathodic peak potential. [e]) Anodic peak potential. [f]) Reversible transfer.

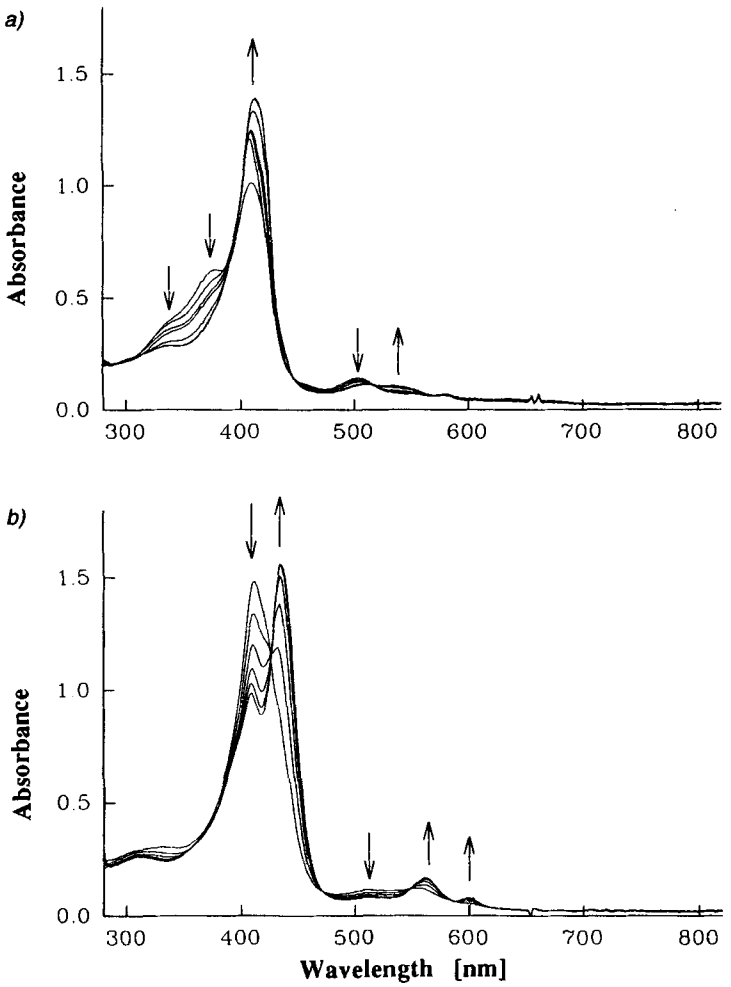

Fig. 7. *Time-resolved UV/VIS spectroelectrochemistry on an OTTLE in* CH_2Cl_2 (+ 0.1M Bu_4NPF_6) *upon controlled-potential reduction of* **4 · FeCl** *at* a) *−0.9 V* vs. *SCE* (first reduction step) *and* b) *at −1.6 V* vs. SCE (second reduction step)

2.3.3. *Electrochemical Studies of* **4 · FeCl** *and* **5 · FeCl** *in Aqueous Solution.* To compare the redox behavior of the dendritic iron porphyrins to that of globular heme proteins such as cytochrome-*c* more directly, cyclic voltammetric studies were carried out in H_2O with 0.1M Et_4NClO_4 as the supporting electrolyte (*Fig. 8*). For solubility reasons (see *Sect. 2.1*), only the dendritic derivatives **4 · FeCl** and **5 · FeCl** could be studied in aqueous solution. They both exhibited irreversible one-electron oxidation steps using a glassy carbon working electrode at potentials of + 0.97 and + 1.09 V *vs.* SCE (*Table 3*). Compounds **4 · FeCl** and **5 · FeCl** also displayed two reduction steps, the second of which was irreversible and occurred at the same potential of −1.26 V *vs.* SCE. In contrast, the fully reversible first reduction step, which corresponds to the Fe^{III}/Fe^{II} couple, was shifted

from −0.23 V *vs.* SCE in **4 · FeCl** to + 0.19 V in **5 · FeCl**. This dramatic shift to more positive (anodic) potential of 420 mV must be caused by the increase in density of the dendritic superstructure and its effect on the environmental polarity around the electrophore.

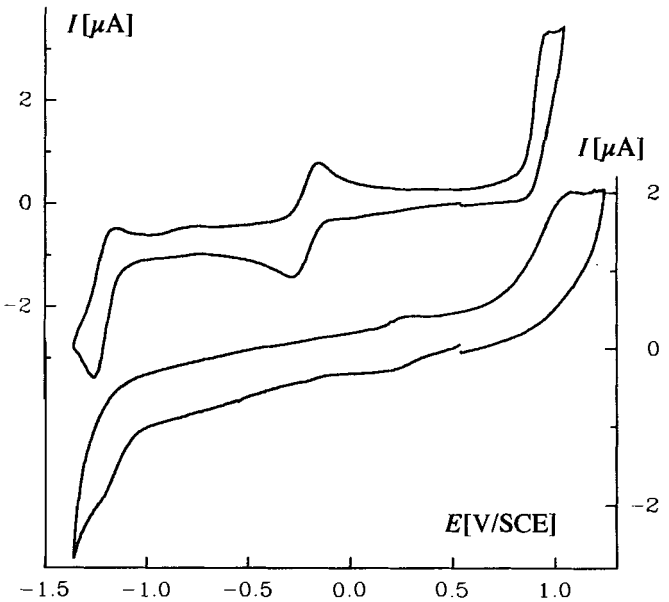

Fig. 8. *Cyclic voltammograms of* **4 · FeCl** (top) *and* **5 · FeCl** (bottom) *in* H_2O (+ 0.1M Et_4NPF_6) *on a glassy carbon working electrode.* Scan rate: 0.05 Vs^{-1}.

Table 3. *Redox Potentials of the Dendritic Iron Porphyrins in* H_2O[a])

Porphyrin	$E_{Fe^{II}/Fe^{I}}$	$E_{Fe^{III}/Fe^{II}}$	E_{ox}
4 · FeCl	−1.26[b])	−0.23[c])	+0.97[b])
5 · FeCl	−1.26[b])	+0.19[c])	+1.09[b])

[a]) Redox potentials in H_2O determined by cyclic voltammetry (CV): E (approximated by $(E_p^a + E_p^c)/2$) in V *vs.* SCE; supporting electrolyte 0.1M Et_4NClO_4; glassy carbon working electrode, scan rate = 0.1 Vs^{-1}, T = 293 K. [b]) Irreversible transfer, peak potential from CV. [c]) Reversible transfer.

In CH_2Cl_2, the iron porphyrins in both the more open **4 · FeCl** and the more densely packed **5 · FeCl**, experience similar microenvironments whose polarity is largely determined by the dendritic branches and not so much by the solvent; hence, the potentials for the Fe^{III}/Fe^{II} couple in the two compounds differ by only 80 mV. In H_2O, however, the iron porphyrin in **4 · FeCl** is solvated by bulk solvent as the relatively open dendritic branches do not impede its access to the central core. In contrast, the more densely packed dendritic superstructure of **5 · FeCl** significantly reduces contact between the heme and external solvent, presumably permitting only access of individual H_2O molecules but not of bulk solvent to the central electrophore. As a result, the oxidized,

more highly charged Fe^{III} state is destabilized relative to Fe^{II} and the redox potential is strongly shifted to a more positive value.

The remarkable potential difference for the Fe^{III}/Fe^{II} couple in **4 · FeCl** and **5 · FeCl** corresponds to the predictions made by the electrostatic model of *Kassner* (see *Sect. 2.3.1*) and resembles those encountered in comparisons between cytochromes and simple H_2O-soluble iron porphyrins [4]. Although this similarity suggests that dendritic porphyrins are close functional mimics of globular heme electron-transfer proteins, further analogies between dendritic and biological systems are currently limited by the difference in axial ligation to the heme iron. The protein cytochrome-*c* has a histidine N-atom and a methionine S-atom as axial ligands, whereas the nature of these ligands in the dendritic systems is not known in aqueous solution. Axial ligands to the metal ion center in the latter systems could include the Cl^- anion, H_2O molecules, or donor atoms from the dendritic branches. Based on the full reversibility of the reduction step from Fe^{III} to Fe^{II}, we can only conclude at present that the same axial ligands remain coordinated during the time scale of the CV experiment. By covalently inserting the natural N- and S-ligands into dendritic iron porphyrins, their ability to model cytochrome-*c* could be further extended, and this objective is now being pursued in our laboratory.

3. Conclusions. – With the dendritic porphyrins **1 · Zn**–**3 · Zn** and **4 · FeCl**/**5 · FeCl**, functional mimics of globular electron-transfer heme proteins were prepared by divergent growth methodology. In these compounds, a dendritic superstructure extending up to 4 nm in diameter (in the third-generation derivative **3 · Zn**) surrounds a central metal porphyrin core. They were obtained using the versatile poly(ether-amide) cascade technology introduced by *Newkome et al.* [23], which relies on highly efficient peptide coupling protocols for attachment of the various generations of dendritic branches. All compounds, including the third-generation derivative **3 · Zn** with a molecular weight of 19054 D, were shown to be pure according to ^{13}C-NMR spectroscopy. Whereas compounds **1 · Zn**–**3 · Zn** with 12, 36, and 108 methyl-carboxylate end groups were highly soluble only in organic solvents, the Fe^{III} derivatives **4 · FeCl** and **5 · FeCl** with 12 and 36 terminal esters of triethyleneglycol monomethyl ether were readily soluble in both organic and aqueous solutions.

Cyclic voltammetry revealed strong microenvironment effects of the dendritic superstructure on redox processes of the core electrophore in both organic and aqueous solutions. Progressing from **1 · Zn** to **3 · Zn** in THF, the first porphyrin-centered oxidation and reduction potentials become more negative by 320 and 210 mV, respectively. With increasing generation, the poly(ether-amide) dendritic shell makes the microenvironment around the central porphyrin ring more electron-rich which, in return, destabilizes the porphyrin radical anion formed upon reduction and stabilizes the porphyrin radical cation formed upon oxidation. Studies with related poly(ether-amide) dendrimers containing cyclophane receptor cores have demonstrated that solutes such as neutral and ionic naphthalene derivatives as well as steroids can penetrate rapidly to the central core, even in third-generation compounds [9 b, c]. Therefore, we exclude the alternative explanation that the potential shifts observed for **1 · Zn**–**3 · Zn** originate from differences in the accessibility of counterions from the electrolyte to the porphyrin core.

In H_2O, cyclic voltammetric studies revealed a dramatic difference between the potential of the Fe^{III}/Fe^{II} couple in **4 · FeCl** and **5 · FeCl** with the potential of the higher-

generation compound being shifted by 420 mV to more positive values. This large shift can be explained by differences in solvation of the core electrophore. Whereas the relatively open dendritic branches in **4 · FeCl** do not impede access of bulk solvent to the central core, the densely packed dendritic superstructure of **5 · FeCl** significantly reduces contact between the heme and external solvent. As a result, the more charged Fe^{III} state is destabilized relative to Fe^{II}, and the redox potential is strongly shifted to a more positive value. Therefore, we view the dendritic iron porphyrin **5 · FeCl** as a valid model for globular heme proteins such as cytochrome-*c*. The iron heme moiety in these electron-transfer proteins exhibits oxidation potentials in aqueous solution 200–400 mV more positive than those of similarly ligated iron heme model systems that lack the hydrophobic peptidic shell. Future investigations still need to address the effects of different axial ligation to the dendritic iron porphyrin on the Fe^{III}/Fe^{II} redox potential.

The described studies validate the model character of dendritic porphyrins such as **5 · FeCl** for globular electron-transfer heme proteins. They also demonstrate a versatile new approach to modulating and optimizing the reduction potential of redox catalysts by controlling the polarity of their environment using dendrimer technology. Attachment of dendritic shells by divergent or convergent growth methods should find increasing future application in tuning the potential of electrophores for use as redox mediators in electrocatalysis or for performing specific tasks in advanced material design [16].

Experimental Part

General. Reagents and solvents were reagent-grade commercials and were used without further purification. THF was freshly distilled from sodium benzophenone ketyl. All reactions were carried out under a positive pressure of N_2 unless otherwise specified, and all manipulations with porphyrins were conducted in the dark. Evaporation *in vacuo* was done at water aspirator pressure; if not stated otherwise, isolated solid products were dried in vacuum at 0.1 Torr. Column chromatography: SiO_2-*60* (230–400 mesh, 0.040–0.063 mm) from *E. Merck*. TLC: plastic sheets pre-coated with SiO_2-*G* UV_{254} from *Macherey-Nagel* and glass-backed SiO_2-*60* F_{254} from *Merck*; visualization by UV light. Preparative gel permeation chromatography (GPC): *Biobeads SX-3* (exclusion limit 2000 Da) or *Biobeads SX-1* (fractionation range 600–1400 Da) from *Biorad*. If not stated otherwise, GPC was done on columns of 3 cm diameter and 100 cm length. M.p.: *Büchi Smp-20*; uncorrected. UV/VIS Spectra: *Varian Cary-5* spectrophotometer; λ_{max} in nm (log ε). IR Spectra [cm^{-1}]: *Perkin-Elmer 1600-FTIR*. NMR Spectra: *Bruker AM 500* (^{13}C) and *Varian Gemini 300* or *200* (^1H) at 296 or 300 K, with Me_4Si or solvent peaks ($CHCl_3$ = 7.26 (^1H) and 77.0 (^{13}C)) as reference. MALDI-TOF-MS (*m/z* (%)): *Bruker REFLEX* spectrometer with 2,4,6-trihydroxyacetophenone (THA) or α-cyano-4-hydroxycinnamic acid (CCA) as matrix; positive-ion mode. If not indicated otherwise, samples were prepared by mixing 1 μl of a soln. of the dendrimer (*ca.* 1 mg ml^{-1}) in CH_2Cl_2 with 1 μl of a soln. of the matrix CCA (0.1M) in MeCN/EtOH/H_2O 50:45:5. A 1 μl sample was then deposited on the probe tip, dried under mild vacuum, and analyzed. FAB-MS (*m/z* (%)): *VG ZAB 2 SEQ* instrument; *3*-nitrobenzyl alcohol as matrix. For MALDI-TOF- and FAB-MS of dendrimers, the experimentally observed highest peak in the molecular ion cluster is reported followed in parenthesis by the calculated isotopic molecular formula. For some compounds, the entire molecular ion cluster is reported with the charged species being assigned by comparison with a simulated spectrum. Elemental analyses were performed by the Mikrolabor at the Laboratorium für Organische Chemie, ETH-Zürich. All cascade molecules were named by the *Chemical Abstracts Service* (*CAS*).

Electrochemistry. Cyclic voltammetric studies in a three-electrode cell were performed in CH_2Cl_2 or THF with 0.1M Bu_4NPF_6 as electrolyte or in H_2O with 0.1M Et_4NPF_6 as electrolyte, at 293 ± 2 K. The experiments were carried out either with a multipurpose electrochemical device *PRG 4* (*Solea Tacussel*) for cyclic voltammetry on a dropping Hg electrode, or, for cyclic voltammetry on Pt or glassy C electrodes, with a *EG & G Princeton Applied Research Potentiostat/Galvanostat* (model 273) in conjunction with the model *273 electrochemical analysis software, V. 2.02, EG & G Instruments, Inc.*, running on a PC. Measurements in CH_2Cl_2 were done on Pt or glassy C working electrodes, in H_2O on a glassy C working electrode, and in THF on a dropping Hg electrode. Ag/AgCl

and SCE were used as reference electrodes. All potentials presented in the present study are given *vs.* SCE, using the ferrocene/ferricinium couple as internal redox standard. At the glassy C electrode, the accessible potential range in CH_2Cl_2 was from *ca.* −2.0 to + 1.3 V, in H_2O from *ca.* −1.6 to + 1.2 V. Spectroelectrochemical studies were carried out in CH_2Cl_2 (+ 0.1M Bu_4NPF_6) on an OTTLE (optically transparent thin layer electrode). The working electrode was a Pt grid (1000 mesh). The spectra were recorded on a *Hewlett-Packard 8452 A* diode array spectrophotometer.

Computer Modeling of Dendrimer **3** · **Zn**. The program *Insight II* (version 2.3.0, *Biosym Technologies, Inc.*, San Diego, CA, 1993) was used for the computer simulation of **3** · **Zn**. Steric clashes in the initial input structure were removed by performing an energy minimization (*DISCOVER, Biosym Technologies*) first with steepest descents and then with conjugate gradient methods to an RMS (= root mean square) gradient of less than 0.1 with the *CVFF* force field. A similar modeling was performed on **5** · $\mathbf{H_2}$ in order to estimate the radius of the dendritic shell for evaluation of the potential of the Fe^{III}/Fe^{II} couple according to *Kassner* [4].

Diethyl 4,4'-[(2-Formyl-1,3-phenylene)bis(oxy)]bis(butanoate) (7). A mixture of 2,6-dihydroxybenzaldehyde [18b] (2.10 g, 15.2 mmol) and K_2CO_3 (8.40 g, 60.8 mmol) in DMF (50 ml) was heated under N_2 to 60° for 1 h. After addition of ethyl 4-bromobutyrate (7.50 g, 38.4 mmol), the mixture was heated to 80° for 2 d, then the inorg. salts were removed by filtration, and the solvent was evaporated. The residual oil was dissolved in CH_2Cl_2, washed with 10% aq. HCl soln., and dried (Na_2SO_4). Evaporation followed by FC (SiO_2, PhMe/AcOEt 9:1) yielded 7 (3.64 g, 65%). Waxy-yellow solid. M.p. 40–41°. IR (KBr): 1730, 1686 (C=O). ^{1}H-NMR (500 MHz, $CDCl_3$): 1.26 (*t*, *J* = 7.2, 6 H); 2.15 (*quint.*, *J* = 6.8, 4 H); 2.56 (*t*, *J* = 6.8, 4 H); 4.09 (*t*, *J* = 6.8, 4 H); 4.14 (*q*, *J* = 7.2, 4 H); 6.55 (*d*, *J* = 8.5, 2 H); 7.39 (*t*, *J* = 8.5, 1 H); 10.52 (*s*, 1 H). ^{13}C-NMR (100 MHz, $CDCl_3$): 13.77; 23.96; 30.12; 60.02; 67.23; 104.41; 114.41; 135.23; 160.91; 172.75; 188.50. FAB-MS: 367 (40, MH$^+$), 115 (100, $C_6H_{11}O_2^+$). Anal. calc. for $C_{19}H_{26}O_7$ (366.4): C 62.28, H 7.15; found: C 62.27, H 7.13.

*Tetraethyl 4,4',4'',4'''-[21*H*,23*H*-Porphine-5,15-diylbis[2,1,3-benzenetriylbis(oxy)]]tetrakis(butanoate)* (**9** · $\mathbf{H_2}$). To a soln. of **7** (0.619 g, 1.69 mmol) and **8** [19] (0.247 g, 1.69 mmol) in dry CH_2Cl_2 (300 ml) was added CF_3CO_2H (5 drops). After stirring at r.t. for 18 h, *o*-chloranil (1.66 g, 6.76 mmol) was added and the mixture heated to reflux for 1 h. After adsorption on SiO_2 by evaporation, chromatography (SiO_2, PhMe/AcOEt 9:1) and recrystallization ($CHCl_3$/MeOH) gave **9** · $\mathbf{H_2}$ (0.359 g, 43%). Shiny-purple crystals. M.p. 150–151°. UV/VIS (CH_2Cl_2): 408 (5.68), 502 (4.22), 535 (3.68), 578 (3.73), 633 (3.05). IR (KBr): 1727 (C=O). ^{1}H-NMR (500 MHz, $CDCl_3$): −3.03 (*s*, 2 H); 0.805 (*t*, *J* = 7.3, 12 H); 1.26 (*quint.*, *J* = 6.0, 8 H); 1.32 (*t*, *J* = 6.0, 8 H); 3.62 (*q*, *J* = 7.3, 8 H); 3.91 (*t*, *J* = 6.0, 8 H); 7.03 (*d*, *J* = 8.5, 4 H); 7.72 (*t*, *J* = 8.5, 2 H); 8.96 (*d*, *J* = 4.4, 4 H); 9.29 (*d*, *J* = 4.6, 4 H); 10.18 (*s*, 2 H). ^{13}C-NMR (100 MHz, $CDCl_3$): 13.42; 23.48; 29.29; 59.35; 67.04; 103.89; 105.20; 110.85; 119.45; 129.99; 130.78; 144.72; 147.20; 159.42; 172.50. FAB-MS: 984 (100, MH$^+$). Anal. calc. for $C_{56}H_{62}N_4O_{12}$ (983.1): C 68.42, H 6.36, N 5.70; found: C 68.35, H 6.19, N 5.43.

*(SP-4-1)-[[Tetraethyl 4,4',4'',4'''-[21*H*,23*H*-Porphine-5,15-diylbis[2,1,3-benzenetriylbis(oxy)]]tetrakis[butanoato]](2−)-N^{21},N^{22},N^{23},N^{24}]zinc* (**9** · **Zn**). A mixture of $Zn(OAc)_2 \cdot 2\,H_2O$ (1.40 g, 6.38 mmol) and **9** · $\mathbf{H_2}$ (0.687 g, 0.700 mmol) in $CHCl_3$/MeOH 1:1 (40 ml) was heated to reflux for 30 min. After evaporation, the residue was dissolved in CH_2Cl_2, and the org. phase was washed with H_2O and dried (Na_2SO_4). Evaporation and chromatography (SiO_2, hexane/AcOEt 3:2), followed by recrystallization ($CHCl_3$/MeOH) afforded **9** · **Zn** (0.687 g, 94%). Bright-pink solid. M.p. 178°. UV/VIS (CH_2Cl_2): 411 (5.61), 501 (3.35) 539 (4.18), 576 (3.45). IR (KBr): 1730 (C=O). ^{1}H-NMR (500 MHz, $CDCl_3$): 0.622 (*t*, *J* = 7.1, 12 H); 0.956 (*t*, *J* = 6.7, 8 H); 1.18 (*quint.*, *J* = 6.7, 8 H); 3.30 (*q*, *J* = 7.1, 8 H); 3.87 (*t*, *J* = 6.7, 8 H); 7.07 (*d*, *J* = 8.5, 4 H); 7.72 (*t*, *J* = 8.5, 2 H); 9.04 (*d*, *J* = 4.3, 4 H); 9.34 (*d*, *J* = 4.3, 4 H); 10.19 (*s*, 2 H). ^{13}C-NMR (100 MHz, $CDCl_3$): 13.17; 23.42; 28.91; 59.10; 67.42; 104.78; 106.05; 111.39; 121.74; 129.55; 131.07; 148.81; 150.02; 159.42; 172.21. FAB-MS: 1045 (100, MH$^+$). Anal. calc. for $C_{56}H_{60}N_4O_{12}Zn$ (1046.5): C 64.27, H 5.78, N 5.35; found: C 64.03, H 5.66, N 5.14.

*(SP-4-1)-4,4',4'',4'''-[[[21*H*,23*H*-Porphine-5,15-diylbis[2,1,3-benzenetriylbis(oxy)]]tetrakis[butanoato]]-(2−)-N^{21},N^{22},N^{23},N^{24}]zinc* (**6** · **Zn**). A soln. of **9** · **Zn** (0.900 g, 0.86 mmol) and Na_2CO_3 (1.0 g, 9.43 mmol) in EtOH/H_2O 2:1 (30 ml) was heated to reflux for 15 h. After evaporation, H_2O (100 ml) was added followed by 0.4M HCl until precipitation of **6** · **Zn** started. The mixture was extracted with AcOEt (3 ×), and the combined org. phases were dried ($MgSO_4$) and evaporated. Recrystallization from acetone yielded **6** · **Zn** (670 mg, 83%). Bright-pink powder. M.p. 244°. UV/VIS (MeOH): 391 (4.46); 411 (5.56); 545 (4.02); 581 (2.27). IR (KBr): 1694 (C=O). ^{1}H-NMR (400 MHz, $(CD_3)_2SO$): 1.16 (*quint.*, *J* = 7.0, 8 H); 1.43 (*t*, *J* = 7.0, 8 H); 3.87 (*t*, *J* = 7.0, 8 H); 7.16 (*d*, *J* = 8.5, 4 H); 7.76 (*t*, *J* = 8.5, 2 H); 8.81 (*d*, *J* = 4.2, 4 H); 9.33 (*d*, *J* = 4.2, 4 H); 10.15 (*s*, 2 H); 11.63 (br. *s*, 4 H). ^{13}C-NMR (100 MHz, $(CD_3)_2SO$): 23.61; 29.11; 66.88; 105.31; 108.65; 111.06; 120.63; 129.95; 130.81; 131.26; 148.36; 149.55; 159.14; 173.71. FAB-MS: 932 (100, M^+). HR-FAB-MS: 933.2244 (M^+, $C_{48}H_{44}N_4O_{12}Zn^+$; calc. 932.2247).

*[[Octamethyl 3,3',3'',3''',3'''',3''''',3'''''',3'''''''-[21*H*,23*H*-porphine-5,15-diylbis[2,1,3-benzenetriylbis[oxy(1-oxo-4,1-butanediyl)imino[2-[(3-ethoxy-3-oxopropoxy)methyl]-2,1,3-propanetriyl]bis(oxy)]]]octakis[propanoato]]-*

(2–)-N²¹,N²²,N²³,N²⁴]zinc (**1 · Zn**). A stirred soln. of **6 · Zn** (0.050 g, 0.0538 mmol), BtOH (0.051 g, 0.377 mmol), and **10** (0.123 g, 0.323 mmol) in dioxane (0.20 ml) was cooled to 0° in an ice bath, and DCC (0.133 g, 0.646 mmol) was added rapidly as a solid. The mixture was warmed to r.t. overnight and, after stirring at r.t. for 43 h, the *N,N'*-dicyclohexylurea was removed by filtration and washed with CH_2Cl_2, until all the red pigment was cleared from the filter. Evaporation *in vacuo* yielded a viscous red oil which was dissolved in AcOEt (0.5 ml) and passed quickly through a plug (SiO_2) eluted with AcOEt to remove baseline contaminations. The red material was subsequently subjected to GPC on *Biobeads SX-3* using PhMe as eluent. Evaporation of the red product fraction *in vacuo* yielded **1 · Zn** (0.10 g, 75%). Viscous red oil. UV/VIS ($c = 9.09 \times 10^{-7}$ M, $CHCl_3$): 415 (5.65), 544 (4.62). IR ($CHCl_3$): 1743, 1672 (C=O). ^{1}H-NMR (300 MHz, $CDCl_3$): 1.04–1.19 (*m*, 4 H, $OCH_2CH_2CH_2CH_2$); 1.21–1.30 (*m*, 4 H, $OCH_2CH_2CH_2CH_2$); 2.17 (*t*, *J* = 6.2, 12 H, OCH_2CH_2); 3.15–3.40 (*m*, 84 H, MeO, CH_2O, $OCH_2CH_2CH_2$); 3.89 (*t*, *J* = 5.4, 4 H, $OCH_2CH_2CH_2CH_2$); 4.87 (*s*, 4 H, NH); 7.04 (*d*, *J* = 8.3, 4 H, *m*-aryl-H); 7.70 (*t*, *J* = 8.3, 2 H, *p*-aryl-H); 9.00 (*d*, *J* = 4.4, 4 H, β_2-H); 9.31 (*d*, *J* = 4.4, 4 H, β_1-H); 10.13 (*s*, 2 H, *meso*-H). ^{13}C-NMR (75 MHz, $CDCl_3$): 24.6; 32.4; 34.4; 51.4; 59.5; 66.7; 67.6; 68.9; 104.9; 105.4; 111.8; 121.1; 129.9; 131.2; 131.6; 148.9; 150.4; 159.8; 171.9; 172.5. FAB-MS: 2379.0 (100, MH^+, $^{12}C_{111}{}^{13}CH_{152}N_8O_{44}{}^{64}Zn$ requires 2378.9).

Dodecahydro-[[3,3',3'',3''',3'''',3''''',3''''''',3'''''''-[21H,23H-porphine-5,15-diylbis[2,1,3-benzenetriylbis[oxy(1-oxo-4,1-butanediyl)imino[2-[(2-carboxyethoxy)methyl]-2,1,3-propanetriyl]bis(oxy)]]]octakis[propanoic Acid]] (14–)-N²¹,N²²,N²³,N²⁴]zincate (12–) (**11 · Zn**). To a soln. of **1 · Zn** (0.117 g, 0.05 mmol) in MeOH (1 ml) was added at 0° 1M LiOH (1.0 ml, 1.0 mmol), and the mixture was stirred at r.t. for 48 h. Acidification with 0.4M HCl until product precipitation started, extraction with AcOEt (3 × 2 ml), drying of the combined org. phases ($MgSO_4$), and evaporation *in vacuo* afforded **11 · Zn** (0.089 g, 81%). An anal. pure solvate containing 3 equiv. of THF was obtained, when the original mixture was saturated with NaCl prior to acidification, the extraction done with THF, and when traces of H_2O were removed by azeotropic distillation with benzene, followed by removal of residual inorg. salts through filtration. Red solid. M.p. 94–95°. UV/VIS ($c = 9.09 \times 10^{-7}$ M, THF): 415 (5.57), 545 (4.11). IR (KBr): 1717, 1639 (C=O). ^{1}H-NMR (500 MHz, D_2O): 1.35–1.44 (*m*, 8 H); 1.45–1.51 (*m*, 8 H); 2.46 (*t*, *J* = 6.2, 24 H); 3.51 (*s*, 24 H); 3.64 (*t*, *J* = 6.2, 24 H); 4.06 (*t*, *J* = 6.0, 8 H); 7.43 (*d*, *J* = 8.6, 4 H); 8.05 (*t*, *J* = 8.6, 2 H); 9.21 (*d*, *J* = 4.4, 4 H); 9.66 (*d*, *J* = 4.4, 4 H); 10.51 (*s*, 2 H). ^{13}C-NMR (125 MHz, (D_8)THF): 25.6; 32.6; 35.1; 60.7; 67.8; 68.4; 69.9; 105.5; 105.9; 112.2; 122.2; 131.7; 132.1; 132.2; 149.9; 151.3; 161.1; 172.6; 173.0. FAB-MS: 2211.1 (100, MH^+; $^{12}C_{98}{}^{13}C_2H_{129}N_8O_{44}{}^{64}Zn$ requires 2211.7). Anal. calc. for $C_{100}H_{128}N_8O_{44}Zn \cdot 3$ THF: C 55.41, H 6.31, N 4.62; found: C 55.57, H 6.40, N 4.88.

[[Octamethyl 13,13',13'',13'''-[21H,23H-Porphine-5,15-diylbis[2,1,3-benzenetriylbis[oxy(1-oxo-4,1-butanediyl)imino]]]tetrakis[13-[7,7-bis[(3-methoxy-3-oxopropoxy)methyl]-5,12-dioxo-2,9,13-trioxa-6-azatetradec-1-yl]-6,6,20,20-tetrakis[(3-methoxy-3-oxopropoxy)methyl]-8,18-dioxo-4,11,15,22-tetraoxa-7,19-diazapentacosanedioato]](2–)-N²¹,N²²,N²³,N²⁴]zinc (**2 · Zn**). To a stirred soln. of **11 · Zn** (0.41 g, 0.18 mmol), BtOH (0.58 g, 4.29 mmol), and **10** (1.4 g, 3.7 mmol) in THF (5 ml) at 0° was added DCC (0.76 g, 3.66 mmol) rapidly as a solid. The mixture was warmed to r.t. overnight and, after stirring for 18 h, the *N,N'*-dicyclohexylurea was removed by filtration and washed with CH_2Cl_2 until all the red pigment was cleared from the filter. Evaporation *in vacuo* provided a viscous red oil which was purified by GPC on *Biobeads SX-1* with PhMe as the eluent. Evaporation *in vacuo* of the product band yielded **2 · Zn** (1.0 g, 83%). Viscous red oil. UV/VIS (9.09×10^{-7} M, $CHCl_3$): 415 (5.54), 545 (4.48). IR ($CHCl_3$): 1733, 1667 (C=O). ^{1}H-NMR (300 MHz, $CDCl_3$): 1.10–1.30 (br. *s*, 4 H, $OCH_2CH_2CH_2CH_2$); 1.40–1.60 (br. *s*, 4 H, $OCH_2CH_2CH_2CH_2$); 1.90–2.20 (br. *s*, 12 H, OCH_2CH_2, first gen.); 2.25–2.50 (br. *s*, 72 H, OCH_2CH_2, second gen.); 3.10–3.60 (*m*, 300 H, CH_2OCH_2, MeO); 3.65–3.85 (br. *s*, 4 H, $OCH_2CH_2CH_2CH_2$); 5.80–6.10 (br. *s*, 16 H, NH); 6.97 (*d*, *J* = 7.9, 4 H, *m*-aryl-H); 7.61 (*t*, *J* = 7.9, 2 H, *p*-aryl-H); 8.85 (*d*, *J* = 4.1, 4 H, β_2-H); 9.18 (*d*, *J* = 4.1, 4 H, β_1-H); 9.98 (*s*, 2 H, *meso*-H). ^{13}C-NMR (75 MHz, $CDCl_3$): 24.5; 32.2; 33.8; 36.8; 51.6; 59.6 (2 ×); 66.6 (2 ×); 67.5; 68.9 (2 ×); 104.6; 105.3; 111.4; 121.2; 129.7; 130.9; 131.4; 148.8; 150.2; 159.6; 170.7; 171.9; 172.3. MALDI-TOF-MS: 6547.3 (100%, M^+; $^{12}C_{289}{}^{13}C_3H_{452}N_{20}O_{140}{}^{66}Zn$ requires 6547.8, 6200 (10).

Hexatriacontahydro-[[13,13',13'',13'''-[21H,23H-porphine-5,15-diylbis[2,1,3-benzenetriylbis[oxy(1-oxo-4,1-butanediyl)imino]]]tetrakis[13-[[3-[[2-(2-carboxyethoxy)-1,1-bis[(2-carboxyethoxy)methyl]ethyl]amino]-3-oxopropoxy]methyl]-6,6,20,20-tetrakis[(2-carboxyethoxy)methyl]-8,18-dioxo-4,11,15,22-tetraoxa-7,19-diazapentacosanedioato]](38–)-N²¹,N²²,N²³,N²⁴]zincate (36–) (**12 · Zn**). To a stirred soln. of **2 · Zn** (1.1 g, 0.17 mmol) in MeOH (12 ml) at 0° was added 1M LiOH (12 ml, 12.0 mmol) within 1 h. After stirring at r.t for 48 h, the soln. was saturated with NaCl, acidified until the beginning of product precipitation, and extracted with THF. Traces of H_2O were removed from the THF soln. by azeotropic distillation with benzene, and residual inorg. salts were eliminated through filtration. Evaporation *in vacuo* gave **12 · Zn** (0.96 g, 96%). Red solid. M.p. 64–65°. UV/VIS (9.09×10^{-7} M, MeOH): 415 (5.52); 545 (4.04). IR (KBr): 1722, 1644 (C=O). ^{1}H-NMR (200 MHz, (D_8)THF): 1.02–1.20 (br. *s*, 8 H); 1.50–1.60 (br. *s*, 8 H); 2.05–2.10 (br. *s*, 24 H); 2.25–2.50 (br. *s*, 72 H); 3.20–3.70

(*m*, 192 H); 3.81–3.97 (br. *s*, 8 H); 6.44–6.70 (br. *s*, 16 H); 7.14 (*d*, *J* = 8.0, 4 H); 7.78 (*t*, *J* = 8.0, 2 H); 9.09 (br. *s*, 4 H); 9.67 (br. *s*, 4 H); 10.90 (*s*, 2 H); 36 COOH protons not visible. ^{13}C-NMR (125 MHz, (D_8)THF): 25.7; 32.8; 35.2; 57.6; 60.9 (2×); 67.8 (2×); 68.4; 69.6; 69.8; 105.4; 106.1; 112.3; 122.2; 130.7; 131.8; 132.0; 149.8; 151.2; 160.9; 172.4; 173.3; 173.9. MALDI-TOF-MS (**12** · **Zn** in THF/H_2O 1:1; matrix: 0.1M CCA in EtOH): 6043.6 (100, M^+; $^{12}C_{253}{}^{13}C_3H_{380}N_{20}O_{140}{}^{66}Zn$ requires 6043.3), 5724 (20). Anal. calc. for $C_{256}H_{380}N_{20}O_{140}Zn$ (6043.31): C 50.88, H 6.34, N 4.64; found: C 50.64, H 6.10, N 4.47.

*[[Octamethyl 20,20′,20″,20‴-[21*H,*23*H-*Porphine-5,15-diylbis[2,1,3-benzenetriylbis[oxy(1-oxo-4,1-butanediyl)-imino]]]tetrakis[13,13,27,27-tetrakis[7,7-bis[(3-methoxy-3-oxopropoxy)methyl]-5,12-dioxo-2,9,13-trioxa-6-aza-tetradec-1-yl]-20-[7,7-bis[7,7-bis[(3-methoxy-3-oxopropoxy)methyl]-5,12-dioxo-2,9,13-trioxa-6-azatetradec-1-yl]-14,14-bis[(3-methoxy-3-oxopropoxy)methyl]-5,12,19-trioxo-2,9,16,20-tetraoxa-6,13-diazaheneicos-1-yl]-6,6,34,34-tetrakis[(3-methoxy-3-oxopropoxy)methyl]-8,15,25,32-tetraoxo-4,11,18,22,29,36-hexaoxa-7,14,26,33-tetraaza-nonatriacontanedioato]](2 –)-N^{21},N^{22},N^{23},N^{24}]zinc* (**3** · **Zn**). To a stirred soln. of **12** · **Zn** (0.175 g, 0.029 mmol), BtOH (0.250 g, 1.85 mmol), and **10** (0.592 g, 1.56 mmol) in 1,4-dioxane (5 ml) at 0° was added DCC (0.322 g, 1.56 mmol) rapidly as a solid. The mixture was warmed to r.t. overnight, and, after stirring for 48 h at r.t., the *N*,*N*′-dicyclohexylurea was removed by filtration and washed with CH_2Cl_2, until all the red pigment was cleared from the filter. Evaporation *in vacuo* provided a viscous red oil which was purified by GPC on *Biobeads SX-3* with PhMe as the eluent. Evaporation of the product fraction *in vacuo* gave **3** · **Zn** (0.291 g, 51%). Viscous red oil. UV/VIS (9.1×10^{-7} M, $CHCl_3$): 415 (5.54), 545 (4.48). IR ($CHCl_3$): 1743, 1672 (C=O). ^{1}H-NMR (500 MHz, $CDCl_3$): 1.62 (br. *s*, 4 H, $OCH_2CH_2CH_2$); 1.94 (br. *s*, 4 H, $OCH_2CH_2CH_2$); 2.30 (br. *s*, 96 H, OCH_2CH_2, first and second gen.); 2.46 (br. *s*, 216 H, OCH_2CH_2, third gen.); 3.35–3.85 (br. *m*, 956 H, $OCH_2CH_2CH_2$, CH_2OCH_2, MeO); 6.05–6.35 (br. *m*, 52 H, NH); 7.07 (*s*, 4 H, *m*-aryl-H); 7.68 (br. *s*, 2 H, *p*-aryl-H); 8.91 (br. *s*, 4 H, β_2-H); 9.20 (br. *s*, 4 H, β_1-H); 10.00 (*s*, 2 H, *meso*-H). ^{13}C-NMR (125 MHz, $CDCl_3$): 23.6; 31.8; 33.7; 36.8; 36.9; 51.5; 59.6 (2×); 59.8; 66.6; 67.3; signal for OCH_2 in core linker arm buried; 67.5; 68.9 (3×); 104.3; 105.3; 111.5; 121.2; 129.8; 130.9; 131.4; 148.7; 150.1; 159.3; 170.6; 170.9; 171.9; signal for amide C=O in core linker arm buried. MALDI-TOF-MS (**3** · **Zn** (5×10^{-5}M) in EtOH; matrix: 0.5M THA in EtOH together with 0.1M ammonium citrate in H_2O): 18900 (100, M^+; $^{12}C_{822}{}^{13}C_{10}H_{1352}N_{56}{}^{16}O_{427}{}^{18}O^{64}Zn$ requires 19052).

*4,4′,4″,4‴-[21*H,*23*H-*Porphine-5,15-diylbis[2,1,3-benzenetriylbis(oxy)]]tetrakisbutanoic Acid* (**6** · $\mathbf{H_2}$). A mixture of **9** · $\mathbf{H_2}$ (0.166 g, 0.169 mmol) and Na_2CO_3 (0.150 g, 1.42 mmol) in EtOH/H_2O 1:1 (20 ml) was heated to reflux for 2 d. The volume was reduced by half through evaporation, and the soln. was diluted with H_2O (50 ml). The aq. layer was extracted with CH_2Cl_2 and then brought to pH 5 with conc. aq. HCl. The aq. layer was extracted with AcOEt, and the org. layer was dried (Na_2SO_4) and evaporated to give **6** · $\mathbf{H_2}$ (0.138 g, 94%). Dark-purple solid. M.p. 255–256°. UV/VIS (MeOH): 406 (5.56), 501 (4.18), 533 (3.65), 574 (3.71), 629 (2.99). IR (KBr): 1706 (C=O). ^{1}H-NMR (500 MHz, CD_3OD): 1.20–1.30 (*m*, 16 H); 1.29 (*s*, 2 H); 3.98 (*t*, *J* = 5.63, 8 H); 7.17 (*d*, *J* = 8.6, 4 H); 7.81 (*t*, *J* = 8.6, 2 H); 8.96 (*d*, *J* = 4.5, 4 H); 9.42 (*d*, *J* = 4.5, 4 H); 10.32 (*s*, 2 H). FAB-MS: 871 (100, MH^+). HR-FAB-MS: 871.31905 (M^+; $C_{48}H_{46}N_4O_{12}$, calc. 871.31820).

*[[Tetrakis[2-[2-(2-methoxyethoxy)ethoxy]ethyl 4,4′,4″,4‴-[21*H,*23*H-*Porphine-5,15-diylbis[2,1,3-benzene-triyltetrakis(oxy)]]tetrakis[butanoato]](2 –)-N^{21},N^{22},N^{23},N^{24}]zinc* (**13** · **Zn**). DCC (0.390 g, 1.9 mmol) was added rapidly to a stirred soln. of **6** · **Zn** (0.300 g, 0.32 mmol), BtOH (0.300 g, 2.22 mmol), collidine (1 drop), and triethyleneglycol monomethyl ether (1.20 ml, 7.7 mmol) in freshly distilled THF (1.2 ml) held at 0° in an ice bath. The mixture was stirred for 2 d at r.t., then filtered through cotton wool and evaporated to give a red oil which was passed with $CHCl_3$ through a plug (SiO_2, 1.5-cm diameter, 2-cm length) to remove baseline contaminations. Evaporation afforded a red oil which was again filtered through cotton wool with PhMe, then purified by GPC on *Biobeads SX-1* (2 × 100 cm, drop rate *ca.* 2 ml/min) with PhMe. The front and tail of the red product band were discarded, and evaporation yielded **13** · **Zn** (0.360 g, 74%). Viscous deep-red oil. UV/VIS ($c = 9.09\times10^{-7}$ M, $CHCl_3$): 394 (sh, 4.60), 415 (5.68), 545 (4.17). IR ($CHCl_3$): 1728 (C=O). ^{1}H-NMR (200 MHz, $CDCl_3$): 1.18–1.34 (*m*, 4 H, $OCH_2CH_2CH_2$); 1.36–1.48 (*m*, 4 H, $OCH_2CH_2CH_2$); 2.58–2.65 (*m*, 8 H, triethyleneglycol); 2.68–2.74 (*m*, 20 H, triethyleneglycol, MeO); 2.80–2.92 (*m*, 16 H, triethyleneglycol); 3.03–3.08 (*m*, 8 H, triethyleneglycol); 3.62–3.68 (*m*, 8 H, triethyleneglycol); 3.90 (*t*, *J* = 5.8, 4 H, $OCH_2CH_2CH_2$); 7.05 (*d*, *J* = 8.4, 4 H, *m*-aryl-H); 7.70 (*t*, *J* = 8.4, 2 H, *p*-aryl-H); 9.00 (*d*, *J* = 4.4, 4 H, β_2-H); 9.32 (*d*, *J* = 4.4, 4 H, β_1-H); 10.14 (*s*, 2 H, *meso*-H). ^{13}C-NMR (75 MHz, $CDCl_3$): 23.6; 29.4; 58.0; 62.5; 67.1; 68.2; 69.3; 69.4; 69.7; 70.8; 77.0; 104.6; 105.2; 111.0; 121.2; 129.5; 131.1; 148.7; 150.0; 159.4; 172.3. FAB-MS: 1522.6 (24, M^+; $^{12}C_{74}{}^{13}C_2H_{100}N_4O_{24}{}^{68}Zn$ requires 1522.6), 1521.6 (55, M^+; $^{12}C_{75}{}^{13}CH_{100}N_4O_{24}{}^{68}Zn$ requires 1521.6), 1520.6 (72, M^+; $^{12}C_{76}H_{100}N_4O_{24}{}^{68}Zn$ requires 1520.6), 1519.6 (79, M^+; $^{12}C_{75}{}^{13}CH_{100}N_4O_{24}{}^{66}Zn$ requires 1519.6), 1518.5 (100, M^+; $^{12}C_{76}H_{100}N_4O_{24}{}^{66}Zn$ requires 1518.6), 1517.5 (96, M^+; $^{12}C_{75}{}^{13}CH_{100}N_4O_{24}{}^{64}Zn$ requires 1517.6), 1516.5 (289, M^+; $^{12}C_{76}H_{100}N_4O_{24}{}^{64}Zn$ requires 1516.6).

Tetrakis[2-[2-(2-methoxyethoxy)ethoxy]ethyl] 4,4′,4″,4‴-[21 H,*23* H-*Porphine-5,15-diylbis[2,1,3-benzene-triyltetrakis(oxy)]]tetrakisbutanoic Acid* (**13** · $\mathbf{H_2}$). DCC (1.20 g, 5.81 mmol) was added rapidly to a stirred soln.

of **6** · $\mathbf{H_2}$ (0.420 g, 0.482 mmol), BtOH (0.92 g, 6.81 mmol), collidine (3 drops), and triethyleneglycol monomethyl ether (0.90 ml, 5.79 mmol) in freshly distilled THF (4.0 ml) at 0°. After stirring for 2 d at r.t., the mixture was filtered through cotton wool and evaporated to afford a purple oil which was purified by GPC (*Biobeads SX-1*, PhMe). Evaporation yielded **13** · $\mathbf{H_2}$ (0.50 g, 71%). Viscous dark-purple oil. UV/VIS ($c = 9.09 \times 10^{-7}$ M, $CHCl_3$): 409 (5.44), 504 (4.04), 539 (3.61), 577 (3.61), 632 (3.00). IR ($CHCl_3$): 1728 (C=O). ^{1}H-NMR (300 MHz, $CDCl_3$): −3.13 (*s*, 2 H); 1.21–1.31 (*m*, 8 H); 1.44 (*t*, *J* = 7.1, 8 H); 3.23 (*t*, *J* = 6.4, 8 H); 3.27 (*s*, 12 H); 3.32–3.37 (*m*, 8 H); 3.38–3.44 (*m*, 16 H); 3.45–3.49 (*m*, 8 H); 3.76 (*t*, *J* = 6.0, 8 H); 3.90 (*t*, *J* = 6.0, 8 H); 7.02 (*d*, *J* = 8.4, 4 H); 7.71 (*t*, *J* = 8.4, 2 H); 8.95 (*d*, *J* = 4.5, 4 H); 9.30 (*d*, *J* = 4.5, 4 H); 10.18 (*s*, 2 H). ^{13}C-NMR (75 MHz, $CDCl_3$): 23.9; 29.7; 59.0; 63.1; 67.4; 68.8; 70.4; 70.5; 71.9; 77.7; 104.5; 105.6; 111.3; 119.7; 130.5; 130.6; 131.4; 145.1; 147.6; 159.8; 172.8. FAB-MS: 1457.6 (18, MH$^+$; $^{12}C_{74}{}^{13}C_2H_{103}N_4O_{24}$ requires 1457.7), 1456.5 (56, MH$^+$, $^{12}C_{75}{}^{13}CH_{103}N_4O_{24}$ requires 1455.7), 1455.4 (100, MH$^+$; $^{12}C_{76}H_{103}N_4O_{24}$ requires 1455.7).

Chloro[[tetrakis[2-[2-(2-methoxyethoxy)ethoxy)]ethyl 4,4',4'',4'''-[21 H,*23* H-*Porphine-5,15-diylbis[2,1,3-benzenetriyltetrakis(oxy)]]tetrakis[butanoato]](2−)-*N^{21},N^{22},N^{23},N^{24}*]iron* (**13** · **FeCl**). Anh. $FeCl_2$ (0.925 g, 7.30 mmol) was added to a stirred soln. of **13** · $\mathbf{H_2}$ (0.530 g, 0.363 mmol) in freshly distilled THF (25 ml), and the suspension was heated to reflux for 1 h, then cooled to r.t. After evaporation *in vacuo*, $CHCl_3$ (5 ml) was added and the brown suspension was washed with sat. aq. NaCl soln. (3 × 5 ml), H_2O (5 × 5 ml), and dried ($MgSO_4$). Evaporation provided **13** · **FeCl** (0.50 g, 89%). Brown oil. UV/VIS ($c = 9.09 \times 10^{-7}$ M, $CHCl_3$): 376 (sh, 4.76), 408 (4.99); 502 (4.10), 571 (3.74), 638 (3.60). IR ($CHCl_3$): 1723 (C=O). ^{1}H-NMR (300 MHz, $CDCl_3$): −0.60–6.0 (br. aliphat. signals, *ca.* 84 H); 12.94 (br. *s*, 4 H, β_2-H); 15.03 (br. *s*, 4 H, β_1-H); core *meso*-H (2 H) and aryl-H (6 H) not visible. FAB-MS: 1544.5 (11, M^+; $^{12}C_{76}H_{100}N_4O_{24}{}^{56}$FeCl requires 1544.6), 1510.6 (33, [M − Cl]$^+$; $^{12}C_{75}{}^{13}CH_{100}N_4O_{24}{}^{56}$Fe requires 1510.6), 1509.5 (78, [M − Cl]$^+$; $^{12}C_{76}H_{100}N_4O_{24}{}^{56}$Fe requires 1509.6), 1508.5 (100, [M − Cl]$^+$; $^{12}C_{75}{}^{13}CH_{100}N_4O_{24}{}^{54}$Fe requires 1508.6).

[[Tetrakis[2-[2-(2-methoxyethoxy]ethyl 17,17',17'',17'''-[21 H,*23* H-*Porphine-5,15-diylbis[2,1,3-benzenetriylbis[oxy(1-oxo-4,1-butanediyl)imino]]]tetrakis[12-oxo-17-(5-oxo-2,6,9,12,15-pentaoxahexadec-1-yl)-2,5,8,11,15,19-hexaoxadocosan-22-oato]](2−)-*N^{21},N^{22},N^{23},N^{24}*]zinc* (**4** · **Zn**). DCC (0.390 mg, 1.9 mmol) was added rapidly to a stirred soln. of **11** · **Zn** (0.200 g, 0.09 mmol), BtOH (0.825 g, 6.1 mmol), and collidine (2 drops) in triethyleneglycol monomethyl ether (2.30 ml, 15.0 mmol) at 0°. The mixture was stirred at r.t. for 2 d, then filtered through cotton wool, dissolved in PhMe, filtered, and purified by GPC (*Biobeads SX-1*, PhMe, drop rate 2 ml/min). A single red fraction was collected and evaporated to give **4** · **Zn** (0.389 g, 92%). Viscous deep-red oil. UV/VIS ($c = 9.09 \times 10^{-7}$ M, $CHCl_3$): 395 (4.54); 415 (5.55); 545 (4.16). ^{1}H-NMR (300 MHz, $CDCl_3$): 1.20–1.35 (br. *s*, 4 H, $OCH_2CH_2CH_2$, $OCH_2CH_2CH_2$); 2.34 (*t*, *J* = 6.2, 12 H, OCH_2CH_2); 3.19 (*s*, 12 H, CH_2O); 3.30–3.70 (*m*, 180 H, triethyleneglycol, OCH_3); 3.87 (*t*, *J* = 5.5, 8 H, $OCH_2CH_2CH_2$), 3.97 (*t*, *J* = 4.8, 24 H, triethyleneglycol); 5.35 (*s*, 4 H, NH); 7.05 (*d*, *J* = 8.5, 4 H, *m*-aryl-H); 7.71 (*t*, *J* = 8.5, 2 H, *p*-aryl-H); 9.01 (*d*, *J* = 4.5, 4 H, β_2-H); 9.31 (*d*, *J* = 4.5, 4 H, β_1-H); 10.12 (*s*, 2 H, *meso*-H). ^{13}C-NMR (75 MHz, $CDCl_3$): 24.5; 32.2; 34.6; 58.8; 59.6; 63.4; 66.5; 67.5; 68.9; 69.0; 70.3 (3 ×); 71.7; 104.9; 105.3; 111.8; 121.0; 130.0; 131.3; 131.7; 148.9; 150.3; 159.7; 171.3; 172.4. FAB-MS: 3965 (100, M^+; $^{12}C_{181}{}^{13}C_3H_{296}N_8O_{80}{}^{64}$Zn requires 3964.9).

*Tetrakis[2-[2-(2-methoxyethoxy)ethoxy]ethyl 17,17',17'',17'''-[21*H,*23*H-*Porphine-5,15-diylbis[2,1,3-benzenetriylbis[oxy(1-oxo-4,1-butanediyl)imino]]]tetrakis[12-oxo-17-(5-oxo-2,6,9,12,15-pentaoxahexadec-1-yl-2,5,8,11,15,19-hexaoxadocosan-22-oic Acid]* (**4** · $\mathbf{H_2}$). To a soln. of **4** · **Zn** (0.320 g, 0.081 mmol) in $CHCl_3$ was added 0.4M aq. HCl until the pink mixture turned deep red. The VIS spectrum was inspected qualitatively for appearance of the characteristic four-banded spectrum of a free-base porphyrin between *ca.* 500 and 600 nm. After 30 min, the soln. was washed with 1M aq. Na_2CO_3 soln. (1 ×) and dried ($MgSO_4$). Evaporation *in vacuo* afforded **4** · $\mathbf{H_2}$ (0.290 g, 93%). Viscous dark-purple oil. UV/VIS ($c = 9.09 \times 10^{-7}$ M, $CHCl_3$): 391 (sh, 4.76), 411 (5.46), 504 (4.08), 541 (3.85), 577 (4.04), 633 (2.48). IR ($CHCl_3$): 1733, 1667 (C=O). ^{1}H-NMR (200 MHz, $CDCl_3$): −3.13 (br. *s*, 2 H); 1.15–1.28 (br. *m*, 8 H); 1.29–1.40 (br. *m*, 8 H); 2.42 (*t*, *J* = 6.6, 24 H); 3.26 (*s*, 24 H); 3.35–3.70 (*m*, 180 H); 3.77–3.89 (br. *s*, 8 H); 4.03 (*t*, *J* = 4.4, 24 H); 5.59 (*s*, 4 H); 7.00 (*d*, *J* = 8.6, 4 H); 7.68 (*t*, *J* = 8.6, 2 H); 8.94 (*d*, *J* = 4.8, 4 H); 9.28 (*d*, *J* = 4.8, 4 H); 10.17 (*s*, 2 H). ^{13}C-NMR (75 MHz, $CDCl_3$): 24.6; 32.4; 34.9; 59.2; 59.9; 63.7; 66.9; 67.6; 69.2; 69.3; 70.7 (3 ×); 72.1; 104.5; 105.6; 111.9; 119.4; 131.0 (2 ×); 131.5; 145.2; 147.9; 160.1; 171.8; 172.8. MALDI-TOF-MS: 3902 (100, M^+; $^{12}C_{182}{}^{13}C_2H_{298}N_8O_{80}$ requires 3901.9).

Chloro[tetrakis[2-[2-(2-methoxyethoxy)ethoxy]ethyl 17,17',17'',17'''-[21 H,*23* H-*Porphine-5,15-diylbis-[2,1,3-benzenetriylbis[oxy(1-oxo-4,1-butanediyl)imino]]]tetrakis[12-oxo-17-(5-oxo-2,6,9,12,15-pentaoxahexadec-1-yl)-2,5,8,11,15,19-hexaoxadocosan-22-oato]](2−)-*N^{21},N^{22},N^{23},N^{24}*]iron* (**4** · **FeCl**). Anh. $FeCl_2$ (0.195 g, 1.53 mmol) was added to a stirred soln. of **4** · $\mathbf{H_2}$ (0.300 g, 0.077 mmol) in freshly distilled THF (15 ml), and the suspension was refluxed for 1 h. After evaporation *in vacuo*, $CHCl_3$ (5 ml) was added and the brown suspension

was washed with sat. aq. NaCl soln. (3 × 5 ml), H_2O (5 × 5 ml), and dried ($MgSO_4$). Evaporation *in vacuo* provided **4** · **FeCl** (0.25 g, 85%). Viscous brown oil. UV/VIS ($c = 9.09 \times 10^{-7}$ M, $CHCl_3$): 326 (4.54); 419 (5.11), 504 (4.00), 559 (3.95), 632 (3.24). IR ($CHCl_3$): 1728, 1615 (C=O). ^{1}H-NMR (300 MHz, $CDCl_3$): −0.8–5.9 (br. aliphatic signals, *ca.* 280 H); 13.13 (br. *s*, 4 H, β_2-H); 15.24 (br. *s*, 4 H, β_1-H); core *meso*-H (2 H) and aryl-H (6 H) not visible. MALDI-TOF-MS: 3956.4 (100, $[M - Cl]^+$; $^{12}C_{182}{}^{13}C_2H_{296}N_8O_{80}{}^{56}Fe$ requires 3955.9).

[[Octakis[2-[2-(2-methoxyethoxy)ethoxy]ethyl] 13,13',13'',13'''-[21H,23H-Porphine-5,15-diylbis[2,1,3-benzenetriylbis[oxy(1-oxo-4,1-butanediyl)imino]]]tetrakis[13-[5,12-dioxo-7,7-bis(5-oxo-2,6,9,12,15-pentaoxahexadec-1-yl)-2,9,13,16,19,22-hexaoxa-6-azatricos-1-yl]-8,18-dioxo-6,6,20,20-tetrakis(5-oxo-2,6,9,12,15-pentaoxahexadec-1-yl)-4,11,15,22-tetraoxa-7,19-diazapentacosanedioato]](2−)-N^{21},N^{22},N^{23},N^{24}]zinc (**5** · **Zn**). DCC (0.742 g, 3.6 mmol) was added rapidly to a stirred soln. of **12** · **Zn** (0.300 g, 0.05 mmol), BtOH (0.572 g, 4.23 mmol), and collidine (3 drops) in triethyleneglycol monomethyl ether (1.70 ml, 10.8 mmol) at 0°. After stirring for 2 d at r.t., the mixture was filtered through cotton wool, the solvent was evaporated *in vacuo*, the residue re-dissolved in PhMe, filtered again, and purified by GPC (*Biobeads SX-1*, PhMe, drop rate 2 ml/min). The red product fraction was evaporated *in vacuo* to yield **5** · **Zn** (0.450 g, 80%). Viscous red oil. UV/VIS ($c = 9.09 \times 10^{-7}$ M, $CHCl_3$): 394 (sh, 4.54), 415 (5.67), 545 (4.21). IR ($CHCl_3$): 1733, 1668 (C=O). ^{1}H-NMR (300 MHz, $CDCl_3$): 1.12–1.42 (br. *s*, 4 H, $OCH_2CH_2CH_2$); 1.71–1.83 (br. *s*, 4 H, $OCH_2CH_2CH_2$), 2.45 (br. *s*, 12 H, OCH_2CH_2, first gen.); 2.44–2.60 (br. *s*, 36 H, OCH_2CH_2, second gen.); 3.24–3.75 (*m*, 660 H, dendritic CH_2OCH_2 and triethyleneglycol); 3.80 (br. *s*, 4 H, $OCH_2CH_2CH_2$); 4.14 (br. *s*, 36 H, $CO_2CH_2CH_2$); 6.14–6.26 (br. *s*, 16 H, NH); 7.06 (*d*, *J* = 7.5, 4 H, *m*-aryl-H); 7.69 (*t*, *J* = 7.5, 2 H, *p*-aryl-H); 8.94 (*d*, *J* = 3.9, 4 H, β_2-H); 9.26 (*d*, *J* = 3.9, 4 H, β_1-H); 10.07 (*s*, 2 H, *meso*-H). ^{13}C-NMR (125 MHz, $CDCl_3$): 23.8; 31.8; 34.6; 36.8; 58.7; 59.2 (2×); 63.4; 66.5 (2×); 67.3; 68.8 (2×); 68.9; 70.2; 70.3 (2×); 71.6; 104.5; 105.1; 111.6; 120.7; 129.8; 131.0; 131.5; 148.7; 150.2; 159.5; 170.9; 171.3; 172.0. MALDI-TOF-MS: 11304 (M^+; $^{12}C_{502}{}^{13}C_6H_{884}N_{20}O_{248}{}^{64}Zn$ requires 11303.6), 11248, 10696, 10641.

Octakis[2-[2-(2-methoxyethoxy)ethoxy]ethyl 13,13',13'',13'''-[21H,23H-Porphine-5,15-diylbis[2,1,3-benzenetriylbis[oxy(1-oxo-4,1-butanediyl)imino]]]tetrakis[13-[5,12-dioxo-7,7-bis(5-oxo-2,6,9,12,15-pentaoxahexadec-1-yl)-2,9,13,16,19,22-hexaoxa-6-azatricos-1-yl]-8,18-dioxo-6,6,20,20-tetrakis(5-oxo-2,6,9,12,15-pentaoxahexadec-1-yl)-4,11,15,22-tetraoxa-7,19-diazapentacosanedioic Acid]. (**5** · $\mathbf{H_2}$). Aq. HCl (0.4M) was added slowly to a stirred soln. of **5** · **Zn** (0.211 g, 0.018 mmol) in $CHCl_3$. When the pink soln. turned deep red, the VIS spectrum was inspected qualitatively for the appearance of the characteristic four-banded porphyrin spectrum between *ca.* 500 and 650 nm. The soln. was washed with 1M Na_2CO_3 (2 ml) and dried ($MgSO_4$). Evaporation *in vacuo* afforded **5** · $\mathbf{H_2}$ (0.180 g, 88%). Viscous dark-purple oil. UV/VIS ($c = 9.09 \times 10^{-7}$ M, $CHCl_3$): 391 (sh, 4.83), 411 (5.52), 504 (4.15), 541 (3.90), 577 (3.70), 620 (2.70). IR ($CHCl_3$): 1733, 1667 (C=O). ^{1}H-NMR (300 MHz, $CDCl_3$): −3.13 (br. *s*, 2 H); 1.23–1.46 (br. *s*, 8 H); 1.68–1.85 (br. *s*, 8 H); 2.35 (br. *s*, 24 H); 2.49 (br. *s*, 72 H); 3.20–3.70 (*m*, 660 H); 3.79 (br. *s*, 8 H); 4.14 (br. *s*, 72 H); 6.06–6.18 (br. *m*, 16 H); 7.05 (*d*, *J* = 8.0, 4 H); 7.68 (*t*, *J* = 8.0, 2 H); 8.92 (*d*, *J* = 4.5, 4 H); 9.25 (*d*, *J* = 4.5, 4 H); 10.12 (*s*, 2 H). ^{13}C-NMR (75 MHz, $CDCl_3$): 23.9; 31.8; 34.7; 37.0; 58.9; 59.7 (2×); 63.5; 66.6 (2×); 67.4; 68.9 (2×); 69.0; 70.4 (3×); 71.8; 104.1; 105.3; 111.5; 118.9; 130.5; 131.1 (2×); 144.7; 147.5; 159.5; 170.9; 171.4; 172.1. MALDI-TOF-MS: 11240 (M^+; $^{12}C_{504}{}^{13}C_4H_{886}N_{20}O_{248}$ requires 11240), 11110, 10623.

Chloro[Octakis[2-[2-(2-methoxyethoxy)ethoxy]ethyl 13,13',13'',13'''-[21H,23H-Porphine-5,15-diylbis[2,1,3-benzenetriylbis[oxy(1-oxo-4,1-butanediyl)imino]]]tetrakis[13-[5,12-dioxo-7,7-bis(5-oxo-2,6,9,12,15-pentaoxahexadec-1-yl)-2,9,13,16,19,22-hexaoxa-6-azatricos-1-yl]-8,18-dioxo-6,6,20,20-tetrakis(5-oxo-2,6,9,12,15-pentaoxahexadec-1-yl)-4,11,15,22-tetraoxa-7,19-diazapentacosanedioato]](2−)-N^{21},N^{22},N^{23},N^{24}]iron (**5** · **FeCl**). Anh. $FeCl_2$ (0.100 g, 0.78 mmol) was added to a stirred soln. of **5** · $\mathbf{H_2}$ (0.200 g, 0.018 mmol) in freshly distilled THF (5 ml). The suspension was heated to reflux for 1 h, the solvent was removed *in vacuo*, $CHCl_3$ (5 ml) was added to the residue, and the resulting brown suspension was washed with sat. aq. NaCl soln. (3 × 5 ml), H_2O (5 × 5 ml), and dried ($MgSO_4$). Evaporation *in vacuo* provided **5** · **FeCl** (0.160 g, 80%). Viscous brown oil. UV/VIS ($c = 9.09 \times 10^{-7}$ M, $CHCl_3$): 328 (4.59), 411 (4.97), 571 (3.86), 632 (3.34). IR ($CHCl_3$): 1738, 1667 (C=O). ^{1}H-NMR (300 MHz, $CDCl_3$): 1.7–4.5 (extremely br. aliphatic signals), 13.22 (br. *s*, 4 H, β_2-H); 15.25 (br. *s*, 4 H, β_1-H); core *meso*-H (2 H) and aryl-H (6 H) not visible. MALDI-TOF-MS: 11297 ($[M - Cl]^+$, $^{12}C_{502}{}^{13}C_6H_{884}N_{20}O_{248}{}^{56}Fe$ requires 11296), 10701.

This work was supported during its initial stages (UCLA, 1990–92) by the *U.S. Office of Naval Research*, and subsequently by a grant from the *ETH Research Council* and by *F. Hoffmann-La Roche AG*, Basel. We thank Prof. *R. J. M. Liskamp* for valuable advice during his sabbatical stay at UCLA, and Dr. *W. Amrein* for the mass spectra.

REFERENCES

[1] A. J. Kirby, *Angew. Chem.* **1996**, *108*, 771; *ibid. Int. Ed.* **1996**, *35*, 707; Y. Murakami, J. Kikuchi, Y. Hisaeda, O. Hayashida, *Chem. Rev.* **1996**, *96*, 721; R. Breslow, *Acc. Chem. Res.* **1995**, *28*, 146.

[2] P. G. Schultz, R. A. Lerner, *Science (Washington, D.C.)* **1995**, *269*, 1835; J. W. Bryson, S. F. Betz, H. S. Lu, D. J. Suich, H. X. Zhou, K. T. O'Neil, W. F. DeGrado, *ibid.* **1995**, *270*, 935; J. Kyte, 'Mechanism in Protein Chemistry', Garland, New York, 1995; M. R. Haynes, E. A. Stura, D. Hilvert, I. A. Wilson, *Science (Washington, D.C.)* **1994**, *263*, 646; A. Fersht, 'Enzyme Structure and Mechanism', 2nd edn., Freeman, New York, 1985.

[3] For some recent examples, see: H.-A. Wagenknecht, W.-D. Woggon, *Angew. Chem.* **1997**, *109*, 404; *ibid. Int. Ed.* **1997**, *36*, 390; J. Kang, J. Rebek, Jr., *Nature (London)* **1997**, *385*, 50; P. Mattei, F. Diederich, *Angew. Chem.* **1996**, *108*, 1434; *ibid. Int. Ed.* **1996**, *35*, 1341; A. J. Kennan, H. W. Whitlock, *J. Am. Chem. Soc.* **1996**, *118*, 3027; M.-S. Muche, M. W. Göbel, *Angew. Chem.* **1996**, *108*, 2263; *ibid. Int. Ed.* **1996**, *35*, 2126.

[4] R. J. Kassner, *J. Am. Chem. Soc.* **1973**, *95*, 2674.

[5] D. A. Tomalia, A. M. Naylor, W. A. Goddard, III, *Angew. Chem.* **1990**, *102*, 119; *ibid. Int. Ed.* **1990**, *29*, 138.

[6] G. R. Newkome, C. N. Moorefield, F. Vögtle, 'Dendritic Molecules, Concepts, Syntheses, Perspectives', VCH, Weinheim, 1996.

[7] D. Zanini, R. Roy, *J. Am. Chem. Soc.* **1997**, *119*, 2088; P. R. Ashton, S. E. Boyd, C. L. Brown, N. Jayaraman, J. F. Stoddart, *Angew. Chem.* **1997**, *109*, 756; *ibid. Int. Ed.* **1997**, *36*, 732; T. K. Lindhorst, *Nachr. Chem. Tech. Lab.* **1996**, *44*, 1073; W. T. S. Huck, F. C. J. M. van Veggel, D. N. Reinhoudt, *Angew. Chem.* **1996**, *108*, 1304; *ibid. Int. Ed.* **1996**, *35*, 1213; W. T. S. Huck, F. C. J. M. van Veggel, B. L. Kropman, D. H. A. Blank, E. G. Keim, M. M. A. Smithers, D. N. Reinhoudt, *J. Am. Chem. Soc.* **1995**, *117*, 8293; M. Slany, M. Bardaji, M.-J. Casanove, A.-M. Caminade, J.-P. Majoral, B. Chaudret, *ibid.* **1995**, *117*, 9764; Y.-H. Liao, J. R. Moss, *Organometallics* **1995**, *14*, 2130; Z. Xu, J. S. Moore, *Acta Polymerica* **1994**, *45*, 83; M. R. Bryce, W. Devonport, A. J. Moore, *Angew. Chem.* **1994**, *106*, 1862; *ibid. Int. Ed.* **1994**, *33*, 1761; P. Singh, F. Moll, S. H. Lin, C. Ferzli, K. S. Yu, R. K. Koski, R. G. Saul, P. Cronin, *Clin. Chem.* **1994**, *40*, 1845; J. F. G. A. Jansen, E. M. M. de Brabander-van den Berg, E. W. Meijer, *Science (Washington, D.C.)* **1994**, *266*, 1226; F. Moulines, L. Djakovitch, R. Boese, B. Gloaguen, W. Thiel, J.-L. Fillaut, M.-H. Delville, D. Astruc, *Angew. Chem.* **1993**, *105*, 1132; *ibid. Int. Ed.* **1993**, *32*, 1075; R. Roy, D. Zanini, S. J. Meunier, A. Romanowska, *J. Chem. Soc., Chem. Commun.* **1993**, 1869; C. J. Hawker, J. M. J. Fréchet, *J. Chem. Soc., Perkin Trans. 1* **1992**, 2459; K. L. Wooley, C. J. Hawker, J. M. J. Fréchet, *ibid.* **1991**, 1059.

[8] L. L. Miller, R. G. Duan, D. C. Tully, D. A. Tomalia, *J. Am. Chem. Soc.* **1997**, *119*, 1005; I. Tabakovic, L. L. Miller, R. G. Duan, D. C. Tully, D. A. Tomalia, *Chem. Mater.* **1997**, *9*, 736; J. S. Moore, *Curr. Opin. Solid State Mater. Sci.* **1996**, *1*, 798; S. Stevelmans, J. C. M. van Hest, J. F. G. A. Jansen, D. A. F. J. van Boxtel, E. M. M. de Brabander-van den Berg, E. W. Meijer, *J. Am. Chem. Soc.* **1996**, *118*, 7398; J. K. Young, C. Devadoss, Z. Zhu, P.-W. Wang, J. S. Moore, *Polym. Mater. Sci. Eng.* **1995**, *73*, 224; H. Brunner, *J. Organomet. Chem.* **1995**, *500*, 39; D. Seebach, J.-M. Lapierre, K. Skobridis, G. Greiveldinger, *Angew. Chem.* **1994**, *106*, 457; *ibid. Int. Ed.* **1994**, *33*, 440; D. Seebach, J.-M. Lapierre, G. Greiveldinger, K. Skobridis, *Helv. Chim. Acta* **1994**, *77*, 1673; J. W. J. Knapen, A. W. van der Made, J. C. de Wilde, P. W. N. M. van Leeuwen, P. Wijkens, D. M. Grove, G. van Koten, *Nature (London)* **1994**, *372*, 659; G. R. Newkome, C. N. Moorefield, J. M. Keith, G. R. Baker, G. H. Escamilla, *Angew. Chem.* **1994**, *106*, 701; *ibid. Int. Ed.* **1994**, *33*, 666; S. Achar, R. J. Puddephatt, *Angew. Chem.* **1994**, *106*, 895; *ibid. Int. Ed.* **1994**, *33*, 847; G. R. Newkome, F. Cardullo, E. C. Constable, C. N. Moorefield, A. M. W. C. Thompson, *J. Chem. Soc., Chem. Commun.* **1993**, 925; T. Nagasaki, M. Ukon, S. Arimori, S. Shinkai, *ibid.* **1992**, 608; S. Serroni, G. Denti, S. Campagna, A. Juris, M. Ciano, V. Balzani, *Angew. Chem.* **1992**, *104*, 1540; *ibid. Int. Ed.* **1992**, *31*, 1493.

[9] a) R. J. M. Liskamp, F. Diederich, unpublished results; b) S. Mattei, P. Seiler, F. Diederich, V. Gramlich, *Helv. Chim. Acta* **1995**, *78*, 1904; c) P. Wallimann, P. Seiler, F. Diederich, *ibid.* **1996**, *79*, 779; d) M. Kempfle, P. Wallimann, F. Diederich, unpublished results.

[10] a) P. J. Dandliker, F. Diederich, M. Gross, C. B. Knobler, A. Louati, E. M. Sanford, *Angew. Chem.* **1994**, *106*, 1821; *ibid. Int. Ed.* **1994**, *33*, 1739; b) P. J. Dandliker, F. Diederich, J.-P. Gisselbrecht, A. Louati, M. Gross, *Angew. Chem.* **1995**, *107*, 2906; *ibid. Int. Ed.* **1995**, *34*, 2725; c) J. P. Collman, L. Fu, A. Zingg, F. Diederich, *Chem. Commun.* **1997**, 193.

[11] J. J. Karlsson, T. E. Rostrup, J. Ulstrup, *Acta Chem. Scand.* **1996**, *50*, 284; K. L. Bren, H. B. Gray, *J. Am. Chem. Soc.* **1993**, *115*, 10382; T. Daido, T. Akaike, *J. Electroanal. Chem. Interfacial Electrochem.* **1993**, *344*, 91; M. T. Cruanes, K. K. Rodgers, S. G. Sligar, *J. Am. Chem. Soc.* **1992**, *114*, 9660; S. Komar-Panicucci, J. Bixler, G. Bakker, F. Sherman, G. McLendon, *ibid.* **1992**, *114*, 5443; G. R. Moore, G. W. Pettigrew, 'Cy-

tochromes-*c*: Evolutionary, Structural, and Physicochemical Aspects', Springer, Berlin, 1990, pp. 309–362; K. B. Koller, F. M. Hawkridge, *J. Am. Chem. Soc.* **1985**, *107*, 7412; W. J. Albery, M. J. Eddowes, H. A. O. Hill, A. R. Hillman, *ibid.* **1981**, *103*, 3904; P. K. Warme, L. P. Hager, *Biochemistry* **1970**, *9*, 1606; T. Flatmark, K. Dus, H. deKlerk, M. D. Kamen, *ibid.* **1970**, *9*, 1991.

[12] F. Maltesta, G. Antonini, P. Sarti, M. Brunori, *Biophys. Chem.* **1995**, *54*, 1; H. X. Zhou, *J. Am. Chem. Soc.* **1994**, *116*, 10362; A. M. Bond, *Inorg. Chim. Acta* **1994**, *226*, 293; T. Yagi, *Methods Enzymol.* **1994**, *243*, 104.

[13] J. Issberner, R. Moors, F. Vögtle, *Angew. Chem.* **1994**, *106*, 2507; *ibid. Int. Ed.* **1994**, *33*, 2413.

[14] X. Camps, H. Schönberger, A. Hirsch, *Chem. Eur. J.* **1997**, *3*, 561; S. C. Zimmerman, F. Zeng, D. E. C. Reichert, S. V. Kolotuchin, *Science (Washington, D. C.)* **1996**, *271*, 1095; C. J. Hawker, K. L. Wooley, J. M. J. Fréchet, *J. Am. Chem. Soc.* **1993**, *115*, 4375; K. L. Wooley, C. J. Hawker, J. M. J. Fréchet, F. Wudl, G. Srdanov, S. Shi, C. Li, M. Kao, *ibid.* **1993**, *115*, 9836.

[15] D.-L. Jiang, T. Aida, *Chem. Commun.* **1996**, 1523; R. Sadamoto, N. Tomioka, T. Aida, *J. Am. Chem. Soc.* **1996**, *118*, 3978; Y. Tomoyose, D.-L. Jiang, R.-H. Jin, T. Aida, T. Yamashita, K. Horie, E. Yashima, Y. Okamoto, *Macromolecules* **1996**, *29*, 5236; P. Bhyrappa, J. K. Young, J. S. Moore, K. S. Suslick, *J. Am. Chem. Soc.* **1996**, *118*, 5708; K. W. Pollak, J. W. Leon, J. M. J. Fréchet, *Polym. Mater. Sci. Eng.* **1995**, *73*, 333; R.-H. Jin, T. Aida, S. Inoue, *J. Chem. Soc., Chem. Commun.* **1993**, 1260.

[16] M. R. Bryce, W. Devonport, *Adv. Dendrit. Macromol.* **1996**, *3*, 115; G. Denti, S. Campagna, V. Balzani, *Struct. Energ. React. Chem. Ser., 1 (Mesomolecules)* **1995**, 69; V. Balzani, S. Campagna, G. Denti, A. Juris, S. Serroni, M. Venturi, *Coord. Chem. Rev.* **1994**, *132*, 1.

[17] a) C. Valério, J.-L. Fillaut, J. Ruiz, J. Guittard, J.-C. Blais, D. Astruc, *J. Am. Chem. Soc.* **1997**, *119*, 2588; b) J. Losada, I. Cuadrado, M. Morán, C. M. Casado, B. Alonso, M. Barranco, *Anal. Chim. Acta* **1997**, *338*, 191; c) C.-F. Shu, H.-M. Shen, *J. Mater. Chem.* **1997**, *7*, 47; d) V. V. Narayanan, G. R. Newkome, L. Echegoyen, E. Pérez-Cordero, *Polym. Prepr. Am. Chem. Soc., Div. Polym. Chem.* **1996**, *37* (2), 419; e) H.-F. Chow, I. Y.-K. Chan, D. T. W. Chan, R. W. M. Kwok, *Chem. Eur. J.* **1996**, *2*, 1085; f) A. Juris, M. Venturi, L. Pontoni, A. R. Resino, V. Balzani, S. Serroni, S. Campagna, G. Denti, *Can. J. Chem.* **1995**, *73*, 1875; g) G. R. Newkome, R. Güther, C. N. Moorefield, F. Cardullo, L. Echegoyen, E. Pérez-Cordero, H. Luftmann, *Angew. Chem.* **1995**, *107*, 2159; *ibid. Int. Ed. Engl.* **1995**, *35*, 2023; h) B. Alonso, M. Morán, C. M. Casado, F. Lobete, J. Losada, I. Cuadrado, *Chem. Mater.* **1995**, *7*, 1440; i) S. Campagna, G. Denti, S. Serroni, A. Juris, M. Venturi, V. Ricevuto, V. Balzani, *Chem. Eur. J.* **1995**, *1*, 211.

[18] a) R. Adams, J. Mathieu, *J. Am. Chem. Soc.* **1948**, *70*, 2120; b) R. W. Wagner, J. S. Lindsey, I. Turowska-Tyrk, W. R. Scheidt, *Tetrahedron* **1994**, *50*, 11097.

[19] R. Chong, P. S. Clezy, A. J. Liepa, A. W. Nichol, *Aust. J. Chem.* **1969**, *22*, 229.

[20] J. S. Manka, D. S. Lawrence, *Tetrahedron Lett.* **1989**, *30*, 6989.

[21] M. Nappa, J. S. Valentine, *J. Am. Chem. Soc.* **1978**, *100*, 5075; M. Gouterman, in 'The Porphyrins', Ed. D. Dolphin, Academic Press, New York, 1978, Vol. II, pp. 45–85.

[22] J. E. Baldwin, M. J. Crossley, T. Klose, E. A. O'Rear (III), M. K. Peters, *Tetrahedron* **1982**, *38*, 27; D. R. Benson, R. Valentekovich, S.-W. Tam, F. Diederich, *Helv. Chim. Acta* **1993**, *76*, 2034.

[23] G. R. Newkome, X. Lin, *Macromolecules* **1991**, *24*, 1443; G. R. Newkome, X. Lin, C. D. Weis, *Tetrahedron: Asymmetry* **1991**, *2*, 957; G. R. Newkome, X. Lin, J. K. Young, *Synlett* **1992**, 53.

[24] T. Takano, O. B. Kallai, R. Swanson, R. E. Dickerson, *J. Biol. Chem.* **1973**, *248*, 5234; N. Tanaka, T. Yamane, T. Tsukihara, T. Ashida, M. Kudoko, *J. Biochem. (Tokyo)* **1975**, *77*, 147.

[25] C. Reichardt, 'Solvents and Solvent Effects in Organic Chemistry', 2nd edn., VCH, Weinheim, 1988.

[26] J.-H. Fuhrhop, K. M. Kadish, D. G. Davis, *J. Am. Chem. Soc.* **1973**, *95*, 5140.

[27] C. Gueutin, D. Lexa, M. Momenteau, J.-M. Savéant, F. Xu, *Inorg. Chem.* **1986**, *25*, 4294.

[28] J.-H. Fuhrhop, in 'Porphyrins and Metalloporphyrins', Ed. K. M. Smith, Elsevier, Amsterdam, 1964, pp. 593–623.

[29] K. M. Kadish, M. A. Morrison, L. A. Constant, L. Dickens, D. G. Davis, *J. Am. Chem. Soc.* **1976**, *98*, 8387; H. J. Callot, A. Giraudeau, M. Gross, *J. Chem. Soc., Perkin Trans 2* **1975**, 1321.

[30] H. A. Harbury, P. A. Loach, *J. Biol. Chem.* **1960**, *235*, 3640; J. Shack, W. M. Clark, *ibid.* **1947**, *171*, 143; H. A. Harbury, J. R. Cronin, M. W. Fanger, T. P. Hettinger, A. J. Murphy, Y. P. Myer, S. N. Vinogradov, *Proc. Natl. Acad. Sci. USA* **1965**, *54*, 1658; K. M. Kadish, L. A. Bottomley, *Inorg. Chem.* **1980**, *18*, 832; J. C. Marchon, T. Mashiko, C. A. Reed, in 'Electron Transport and Oxygen Utilization', Ed. C. Ho, Elsevier, North Holland, 1982, pp. 67–72.

[31] A. L. Raphael, H. B. Gray, *J. Am. Chem. Soc.* **1991**, *113*, 1038; A. L. Raphael, H. B. Gray, *Proteins: Struct., Funct., Genet.* **1989**, *6*, 338; V. T. Taniguchi, W. R. Ellis, Jr., V. Cammarata, J. Webb, F. C. Anson, H. B. Gray, *Adv. Chem. Ser.* **1982**, *201*, 51.

[32] K. K. Rodgers, S. G. Sligar, *J. Am. Chem. Soc.* **1991**, *113*, 9419; A. Valiotti, A. Adeyemo, R. F. X. Williams, L. Ricks, J. North, P. Hambright, *J. Inorg. Nucl. Chem.* **1981**, *43*, 2653.
[33] R. Quinn, J. Mercer-Smith, J. N. Burstyn, J. S. Valentine, *J. Am. Chem. Soc.* **1984**, *106*, 4136.
[34] D. Rosen, *Trans. Faraday Soc.* **1963**, *59*, 2178; S. Takashina, H. P. Schwan, *J. Phys. Chem.* **1965**, *69*, 4176.
[35] 'Handbook of Chemistry and Physics', 65th edn., Ed. R. C. West, CRC Press, Boca Raton, 1985, p. E55.
[36] P. J. Dandliker, Ph. D. Dissertation, University of California at Los Angeles, 1995.
[37] D. Lexa, M. Momenteau, P. Rentien, G. Rytz, J.-M. Savéant, F. Xu, *J. Am. Chem. Soc.* **1984**, *106*, 4755; P. Maillard, C. Schaeffer, C. Huel, J.-M. Lhoste, M. Momenteau, *J. Chem. Soc., Perkin Trans. 1* **1988**, 3285; D. Lexa, M. Momenteau, in 'Redox Chemistry and Interfacial Behavior of Biological Molecules', Eds. G. Dryhurst and K. Niki, Plenum, New York, 1988, pp. 1–25.
[38] L. A. Bottomley, K. M. Kadish, *Inorg. Chem.* **1981**, *20*, 1348.